Contrib Mineral Petrol (1999) 134: 380 – 404

Gerhard Vavra · Rolf Schmid · Dieter Gebauer

Internal morphology, habit and U-Th-Pb microanalysis of amphibolite-to-granulite facies zircons: geochronology of the Ivrea Zone (Southern Alps)

Received: 7 July 1998 / Accepted: 4 November 1998

Abstract Several types of growth morphologies and alteration mechanisms of zircon crystals in the high-grade metamorphic Ivrea Zone (IZ) are distinguished and attributed to magmatic, metamorphic and fluid-related events. Anatexis of pelitic metasediments in the IZ produced prograde zircon overgrowths on detrital cores in the restites and new crystallization of magmatic zircons in the associated leucosomes. The primary morphology and Th-U chemistry of the zircon overgrowth in the restites show a systematic variation apparently corresponding to the metamorphic grade: prismatic (prism-blocked) low-Th/U types in the upper amphibolite facies, stubby (fir-tree zoned) medium-Th/U types in the transitional facies and isometric (roundly zoned) high-Th/U types in the granulite facies. The primary crystallization ages of prograde zircons in the restites and magmatic zircons in the leucosomes cannot be resolved from each other, indicating that anatexis in large parts of the IZ was a single and short lived event at 299 ± 5 Ma (95% c. l.). Identical U/Pb ages of magmatic zircons from a metagabbro (293 ± 6 Ma) and a metaperidotite (300 ± 6 Ma) from the Mafic Formation confirm the genetic context of magmatic underplating and granulite facies anatexis in the IZ. The U-Pb age of 299 ± 5 Ma from prograde zircon overgrowths in the metasediments also shows that high-grade metamorphic (anatectic) conditions in the IZ did not start earlier than 20 Ma after the Variscan amphibolite facies metamorphism in the adjacent Strona–Ceneri Zone (SCZ). This makes it clear that the SCZ cannot represent the middle to upper crustal continuation of the IZ. Most parts of zircon crystals that have grown during the granulite facies metamorphism became affected by alteration and Pb-loss. Two types of alteration and Pb-loss mechanisms can be distinguished by cathodoluminescence imaging: zoning-controlled alteration (ZCA) and surface-controlled alteration (SCA). The ZCA is attributed to thermal and/or decompression pulses during extensional unroofing in the Permian, at or earlier than 249 ± 7 Ma. The SCA is attributed to the ingression of fluids at 210 ± 12 Ma, related to hydrothermal activity during the breakup of the Pangaea supercontinent in the Upper Triassic/Lower Jurassic.

(**Abbreviations:** *IZ* Ivrea Zone, *SCZ* Strona Ceneri Zone, *CL* cathodoluminescence, *ZCA* zoning-controlled alteration, *SCA* surface-controlled alteration, *SHRIMP* sensitive high-resolution ion-microprobe)

Introduction

The U-Pb geochronology of high-grade metamorphic terrains relies on zircon and is confronted with conflicting properties of this mineral. On the one hand, zircon crystals are able to accumulate a wealth of chronological information on a number of geological processes. On the other hand, zircons are structurally and morphologically complex, making acquisition and interpretation of the radiometric data difficult. At granulite facies conditions, where other mineral-based radiometric systems are largely reset, due to overstepping of their blocking temperature, zircon keeps at least part of its radiometric memory. As a result, the U-Pb system of many granulite zircons represents complex multi-component mixtures of formation ages. Mixtures of age components within single grains may be generated not only by inheritance, growth and overgrowth of crystals (e.g. Pidgeon and Aftalion 1972), but also by various alteration processes associated with episodic Pb-loss, such as annealing of radiation damage (e.g. Silver

G. Vavra (✉)
Institut für Mineralogie, Universität Tübingen,
D-72074 Tübingen, Germany;
e-mail: gerhard.vavra@uni-tuebingen.de

R. Schmid · D. Gebauer
Departement Erdwissenschaften,
Eidgenössische Technische Hochschule Zürich,
CH-8092 Zürich, Switzerland

Editorial responsibility: J. Hoefs

and Deutsch 1963; Pidgeon et al. 1966; Gebauer and Grünenfelder 1976), recrystallization of unmetamict zircon (e.g. Black et al. 1986; Schiotte et al. 1989; Pidgeon 1992) and leaching of crystals by fluids of special compositions (e.g. Hansen and Friderichsen 1989; Sinha et al. 1992).

Although the microanalytical resolution of age components in structurally complex zircons has become possible by use of the sensitive high-resolution ion-microprobe (SHRIMP; e.g. Williams 1992), reliable interpretation of data is still impeded, because too simplistic conceptions of U-Pb zircon dating are commonly applied. One, that has originated from the observation of Silver and Deutsch (1963), is the general belief that crystal damage induced by radiation is always among the most important factors causing Pb-loss. Accordingly, zircon dating of metamorphic events is considered to be of little reliability, as far as it is based on Pb-loss alone and is not supported by independent geological evidence (e.g. Heaman and Parrish 1991). On the other hand, zircons that grow during high-grade metamorphism and have lower U concentrations and lower radiation damage than typical magmatic crystals are thought to be less prone to Pb-loss, for some considerable time after the high-grade metamorphic event (e.g. Mezger and Krogstad 1997). However, evidence of a mechanism of Pb-loss that appears largely to be independent of radiation damage has been raised by several investigators using the microanalytical technique (e.g. Black et al. 1986; Schiotte et al. 1989; Pidgeon 1992). It is the major purpose of the present paper to distinguish, by internal morphology, Th-U chemistry and U-Pb isotopic data, between different types of zircon growth and alteration mechanisms and to attribute them, as far as possible, to specific environmental ingredients (temperature, fluid infiltration, anatexis) during evolution of the high-grade metamorphic Ivrea Zone.

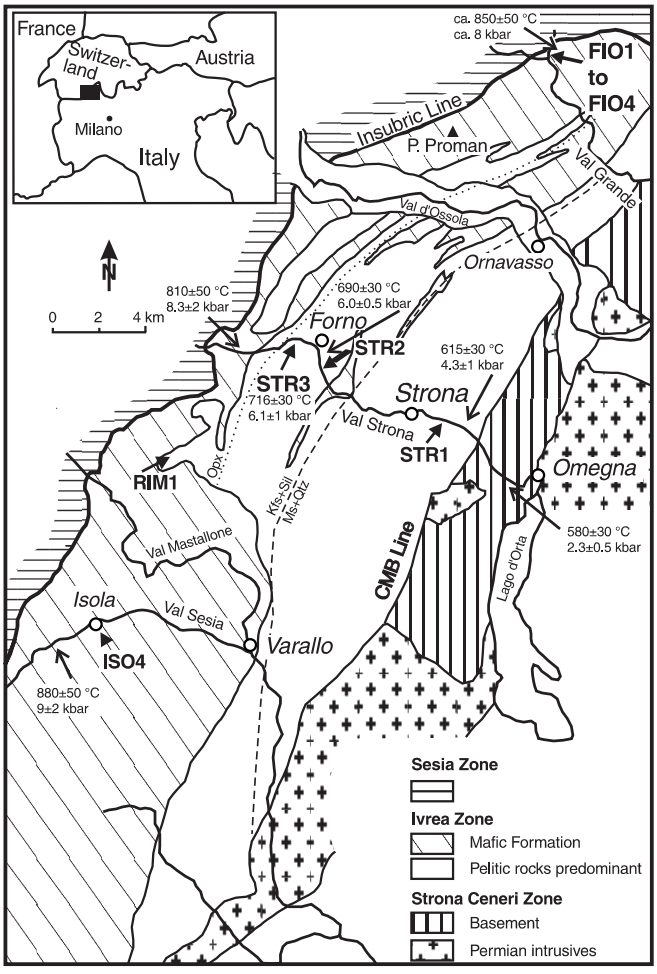

Fig. 1 Sample localities, major lithologies and metamorphic zoning in the Ivrea Zone. Geological boundaries after Zingg (1983). Metamorphic isograds after Zingg (1980). Geothermo- and geobaro-metric data after Sills (1984), Henk et al. (1997) and Rivalenti et al. (1997)

Geological background

The Ivrea Zone (IZ) represents an uptilted part of pre-Alpine lower continental crust exposed between two major fault zones, the Insubric Line of Oligocene age in the northwest and the CMB Line (Boriani et al. 1990) in the southeast, active in the early Permian, but reactivated also in later times (Fig. 1). The southeastern and originally the upper part of the tilted crustal block largely consists of metasediments with intercalations of metabasic rocks. A large concentration of mafic to ultramafic rocks, containing also intercalations of metasediments, is located in what was originally the lower part of the IZ near the Insubric Line, in the so called Mafic Formation. The metamorphic grade in the IZ increases from upper amphibolite facies in the SE to granulite facies in the NW, with peak metamorphic conditions ranging between 600 °C at 4 kbar and 900 °C at 9 kbar (Zingg 1983; Sills 1984; Vogler 1992; Henk et al. 1997; Rivalenti et al. 1997; Stucki 1998). The high-grade metamorphism in the IZ caused large-scale anatectic melting in the quartz-feldspar rocks and produced restites and leucosomes. Most of the anatectic melt was extracted from the complex leaving behind large volumes of restites (Mehnert 1975; Schmid 1978; Schnetger 1994).

The geological evolution of the IZ is presently understood as follows. According to Sills and Tarney (1984), the metasedimentary pile of the IZ with its intercalations of MORB-type basic rocks originated and became strongly deformed in an accretionary prism. When and by which process the rocks of the IZ became buried and finally emplaced at a depth of 30 km is unknown. We only know that at this depth they got intruded by large volumes of mantle magmas (magmatic underplating). These intrusions are thought to have caused the high-grade metamorphic and anatectic climax in the IZ (e.g. Schmid 1967; Schmid and Wood 1976; Pin 1990; Henk et al. 1997). There is now general agreement, based on a very small number of reliable radiometric data, that the major pulse of magmatic underplating occurred in the Late Carboniferous to Early Permian (e.g. Pin 1990; Gebauer 1993), when a transtensional geotectonic regime initiated after the Variscan collision (Handy and Zingg 1991).

The presence of discrete high-temperature extensional shear zones (Brodie and Rutter 1987; Rutter et al. 1993) in combination with radiometric cooling ages (e.g. Brodie et al. 1989) indicates that the exhumation of the IZ, by extensional unroofing, had started already in the Permian. Tectonic and volcanic evidence in the upper crust and sedimentary cover of the Southern Alps (e.g. Bertotti 1991; Bertotti et al. 1993) indicate that continental rifting, giving rise to further exhumation of the IZ, started in the Late Triassic. In the IZ itself, the most obvious expression of this Late Triassic to

Early Jurassic event is the formation of pegmatitic oligoclasite dykes found in the ultramafic and mafic granulite facies rocks (Stähle et al. 1990; Oppizzi and Schaltegger in press). In dykes that have been deformed after their crystallization, plagioclase recrystallized dynamically. Therefore ambient temperatures of higher than 500 °C during or after formation of the pegmatite dykes are suggested. This means that the granulite facies complex was still or again at high temperatures in the Late Triassic or Early Jurassic. The IZ cooled below 300 °C at around 180 Ma (see compilation of Rb-Sr and K-Ar biotite ages in Zingg 1983; Boriani et al. 1985; Bürgi and Klötzli 1990; Table 1 of this work). The final exhumation of the IZ occurred during the Alpine orogeny.

Principal geochronological problems

Metamorphic and magmatic climax

The main phase of magmatic underplating and high-grade metamorphism (anatexis) in the IZ, though regarded as a single and short lived event (e.g. Pin 1990), is as yet poorly constrained by a small number of radiometric data from zircons comprising ill-defined lower intercept ages (around 285 Ma) from 3 metasedimentary samples from Val Strona and Val d'Ossola (Köppel 1974) and an upper intercept age (287 ± 5 Ma) from one metadiorite sample of the Mafic Formation in Val Sesia (Pin 1990). Microanalytical dating (296 ± 12 Ma) of the zircon overgrowth in a restitic metapelite (Vavra et al. 1996) was unable to date the metamorphic climax more precisely. A better constraint of the metamorphic (anatectic) and magmatic climax in the IZ, in terms of regional extent and duration, was a major purpose of the present investigation.

Pre-climax history

Due to complete resetting of nearly all mineral-based radiometric systems during post-collisional high-grade metamorphism, the protolith genesis, sedimentation and pre-climax tectono-metamorphic evolution of the IZ is hardly accessible by radiometric methods. The previously applied whole rock methods of the Rb-Sr (Hunziker and Zingg 1980) and Sm-Nd (Pin 1990) systems, that were originally thought to indicate Early Paleozoic anatexis and mafic underplating, cannot be taken as reliable, because it is not guaranteed that the required large-scale homogenization of the initial isotopic systems was accomplished during the magmatic and anatectic processes (cf. Gebauer et al. 1992).

Zircon is capable of retaining pre-climax geochronological information. This was formerly obtained from upper discordia intercept ages (between 2.5 and 1.9 Ga; Köppel 1974) that are, however, difficult to interpret, due to complex mixtures of formation and Pb-loss events. Though largely inaccessible by radiometric dating, there exists structural evidence of several phases of isoclinal folding pre-dating annealing at the metamorphic climax (Zingg 1983). It is tempting to correlate this early tectono-metamorphic evolution of the IZ with the evolution at higher structural levels of the Southern Alpine basement which is much less obscured by post-collisional magmatic underplating and high-grade metamorphism. It has been supposed that the middle crustal continuation of the lower crustal IZ is represented by the Strona–Ceneri Zone (Fig. 1; Zingg 1983; Handy and Zingg 1991) where the thermal effect of post-collisional magmatism is limited to the contact aureoles of the Permian granitoids. Since mineral-based radiometric systems were not pervasively reset, the Variscan and even pre-Variscan tectono-metamorphic evolution is better revealed in the Strona–Ceneri Zone (SCZ) than in the IZ. Monazite ages and lower intercept ages of zircon of around 450 Ma obtained from rocks interpreted to represent anatectic metasediments in the SCZ indicate an Ordovician age of high-grade metamorphism (Köppel and Grünenfelder 1971; Köppel and Sommerauer 1974). An Ordovician U-Pb age for staurolite from the SCZ (Romer and Franz 1998) accords with this interpretation. Boriani and Villa (1997), however, have re-interpreted the Ordovician monazite and zircon data. They believe that these reflect contact metamorphism and hydrothermal activity caused by granitoids intruding non- or only weakly metamorphosed country rocks. On the basis of Ar-Ar hornblende data, they argue that the metamorphic climax in the SCZ occurred only at 342 ± 2 Ma and was of middle amphibolite facies grade. In any case, if the IZ and SCZ formed a continuous crustal section in Variscan or even pre-Variscan times, regional metamorphic events in the middle crust (SCZ) should correspond to events of higher metamorphic grade in the lower crust (IZ), and these are likely to be recognized in the zircon record. Therefore, a further purpose of the present investigation was to search in the zircons of the IZ for evidence of Variscan and pre-Variscan thermal events, thus contributing to the problem of tectonic coherence of the IZ and SCZ, as already discussed by Handy and Zingg (1991).

Post-climax history

Since the metamorphic climax in the IZ exceeded the blocking temperature of most mineral-based radiometric systems, several authors (e.g. Hunziker and Zingg 1980; Voshage et al. 1987; Brodie et al. 1989; Henk et al. 1997) have supposed a sequence of radiomeric data (Table 1) from monazite (U-Pb), garnet (Sm-Nd), hornblende (Ar-Ar) and mica (Rb-Sr and K-Ar) to represent cooling ages of the granulite complex during its exhumation. Recently, Boriani and Villa (1997) have objected to the interpretation of Ar-Ar hornblende data as cooling ages and have explained the range of ages (see Table 1) by local fluid-assisted recrystallization. Similarly, Vavra and Schaltegger (in this volume) argue against the interpretation of monazite data as cooling ages and explain the large range of apparent monazite ages (Table 1) in terms of partial rejuvenation induced by Upper Triassic fluids.

Considering the tectono-magmatic evolution of the upper crust in the Southern Alps with episodes of volcanism during Permian and Triassic and basin formation during Triassic and later rifting (e.g. Ferrara and Innocenti 1974; Bechstädt et al. 1978; Bertotti et al. 1993), distinct thermal and fluid pulses appear to be a more likely scenario than uniform cooling, during the unroofing of the IZ. A number of zircon formation ages in Table 1 point to magmatic and metasomatic events in the IZ during the Permian and Triassic, but these occurrences have only local extent and the ages do not necessarily reflect the tectono-metamorphic evolution at a larger regional scale. In that respect, the present investigation considers the zircon record in the widely distributed metapelites as more informative.

Localities and description of samples

The samples from which new data are presented in this work originate from two areas of the IZ, from the Val Strona and from the Val Fiorina, a side valley of uppermost Val Grande (Fig. 1). The lithologies, protolithic precursors and metamorphic facies are summarized in Table 2. Modal compositions are presented in Table 3 and bulk chemical compositions (XRF) may be obtained from the authors on request.

The samples from Val Strona (STR1, STR2 and STR3) represent the quartzo-feldspathic metasedimentary lithologies predominating in the southeastern and originally higher crustal levels of the IZ (Fig. 1). The samples show anatectic structures consisting of foliated and intricately folded restitic portions (STR1r, STR2r, STR3r) and cm to dm thick late- to post-kinematic leucosome veins (STR1l, STR2l, STR3l). The ratio of modal garnet to biotite increases with metamorphic grade from the upper amphibolite (STR1) over the transitional (STR2) to the granulite facies (STR3). Sample RIM1 is a banded granulite facies metasediment consisting of a pelitic (RIM1p) and an arenitic (RIM1a) layer. This sample was already investigated in the study of Vavra et al. (1996), but the broader spectrum of the present samples demands some reinterpretation of the earlier given results.

Table 1 Representative compilation of post-climax mineral ages in the Ivrea Zone

Dating method	Metamorphic facies	Age (Ma)	Rock type	Locality	Reference
U-Pb monazite	Amphibolite	265–292	Metapelite	Val Strona	Henk et al. (1996)
U-Pb monazite	Amphibolite	280	Metapelite	Candoglia	Ragettli et al. (1992)
U-Pb monazite	Amphibolite	275 ± 2	Metapelite	Val Strona	Köppel (1974)
U-Pb monazite	Granulite	258–285	Metapelite	Val Strona	Henk et al. (1996)
U-Pb monazite	Granulite	275 ± 2	Metapelite	Val Strona	Köppel (1974)
U-Pb monazite	Granulite	271	Metapelite	Val d'Ossola	Ragettli et al. (1992)
Sm-Nd isochron	Granulite	271 ± 22	Metabasite	Val Sesia	Voshage et al. (1987)
Sm-Nd isochron	Granulite	248 ± 8	Metabasite	Val Sesia	Voshage et al. (1987)
Sm-Nd isochron	Granulite	231 ± 23	Metagabbro	Finero	Lu et al. (1997)
Sm-Nd isochron	Granulite	228 ± 4	Metapelite	Finero	Lu et al. (1997)
Sm-Nd isochron	Granulite	227 ± 3	Metapelite	Val Strona	Voshage et al. (1987)
Sm-Nd isochron	Granulite	226 ± 7	Metagabbro	Finero	Lu et al. (1997)
Sm-Nd isochron	Granulite	223 ± 10	Metagabbro	Finero	Lu et al. (1997)
Sm-Nd isochron	Granulite	214 ± 17	Metagabbro	Finero	Lu et al. (1997)
Sm-Nd isochron	Granulite	203 ± 13	Metagabbro	Finero	Lu et al. (1997)
Ar-Ar hornblende	Amphibolite	243 ± 1	Metabasite	Val Strona	Boriani and Villa (1997)
Ar-Ar hornblende	Amphibolite	183 ± 2	Metabasite	Val Cannobina	Boriani and Villa (1997)
Ar-Ar hornblende	Granulite	242 ± 1	Metabasite	Val Strona	Boriani and Villa (1997)
Ar-Ar hornblende	Granulite	217 ± 1	Metabasite	Val Strona	Boriani and Villa (1997)
Ar-Ar hornblende	Granulite	215 ± 5	Metabasite	Val d'Ossola	Brodie et al. (1989)
Ar-Ar hornblende	Granulite	210 ± 5	Metabasite	Val d'Ossola	Brodie et al. (1989)
K-Ar hornblende	Granulite	208 ± 6	Metabasite	Val d'Ossola	McDowell and Schmid (1968)
Rb-Sr muscovite	Amphibolite	252 ± 10	Pegmatite	Candoglia	Hunziker (1974)
Rb-Sr muscovite	Amphibolite	236 ± 10	Pegmatite	Candoglia	Graeser and Hunziker (1968)
Rb-Sr muscovite	Amphibolite	216 ± 9	Pegmatite	Brissago	Jäger et al. (1967)
K-Ar muscovite	Amphibolite	230 ± 9	Pegmatite	Quarona	Hunziker (1974)
Rb-Sr biotite	Granulite	210–190	Metabasite	Val Sesia	Biino and Meisel (1996)
Rb-Sr biotite	Granulite	184 ± 15	Metapelite	Val d'Ossola	Graeser and Hunziker (1968)
Ar-Ar biotite	Granulite	181–177	Metabasite	Val Sesia	Biino and Meisel (1996)
K-Ar biotite	Amphibolite	176 ± 5	Metapelite	Val d'Ossola	McDowell and Schmid (1968)
K-Ar biotite	Amphibolite	171 ± 5	Metapelite	Val d'Ossola	McDowell and Schmid (1968)
Re-Os isochron	Granulite	217 ± 6	Ore mineral	Val Sesia	Biino and Meisel (1996)
Re-Os isochron	Granulite	214 ± 2	Ore mineral	Val Sesia	Biino and Meisel (1996)
U-Pb zircon formation	Granulite	251 ± 2	Albite granite	Val Sesia	Wright and Shervais (1980)
U-Pb zircon formation	Amphibolite	238 ± 1	Metabasite	Ronco	Gebauer (1993)
U-Pb zircon formation	Granulite	225 ± 13	Oligoclasite	Finero	Stähle et al. (1990)
U-Pb zircon formation	Granulite	212.5	Oligoclasite	Finero	P. Oppizzi and U. Schaltegger (personal communication)
U-Pb zircon formation	Granulite	207 ± 5	Chromitite	Finero	von Quadt et al. (1993)
U-Pb zircon formation	Granulite	201.5	Oligoclasite	Finero	A. von Quadt et al. (personal communication)
U-Pb zircon formation	Granulite	198 ± 2	Oligoclasite	Finero	A. von Quadt et al. (personal communication)
U-Pb zircon formation	Granulite	177	Metabasite	Val Sesia	Gebauer (1993)
U-Pb zircon formation	Granulite	31 ± 1.5	Metabasite	Balmuccia	Gebauer et al. (1992)
U-Pb zircon formation	Granulite	26 ± 1	Metabasite	Balmuccia	Gebauer et al. (1992)
U-Pb zircon alteration	Granulite	265 ± 5	Pyroxenite	Val Sesia	Gebauer et al. (1992)
U-Pb zircon alteration	Granulite	230	Metapelite	Val Sesia	Gebauer (1993)
U-Pb zircon alteration	Granulite	230	Metabasite	Val Sesia	Gebauer (1993)

Sample ISO4 from Val Sesia is peculiar among the quartzofeldspathic lithologies of the IZ in that it contains orthopyroxene instead of sillimanite. It was taken from one of several metasedimentary intercalations within the layered metabasic rocks of the Mafic Formation (Rivalenti et al. 1984). The sample has already been investigated by Vavra et al. (1996) and its protolith interpreted as a calcalkaline intrusive or volcanic to volcaniclastic rock of high-K andesitic to trachyandesitic composition, contaminated by a sedimentary (pelitic) component. The sample is also reconsidered in the broader context of the present study.

Table 2 Sample localities and lithologies

Sample	Lithology	Protolith	Metamorphic facies	Description of locality	Coordinates (*I* Italian, *CH* Swiss)
STR1r	Sil-Bt-gneiss	Pelite	Upper amphibolite	Val Strona 1 km ESE of Strona 200 m E of Ponte Romano, outcrop at southern road side	50050/83860 (I)
STR1l	Qtz-feldspar-gneiss	Granitic leucosome			
STR2r	Pl-Bt-gneiss	Pelite	Transitional to granulite	Val Strona 1 km S of Forno, between Rosarolo and Grampi, outcrop at eastern road side	45340/86200 (I)
STR2l	Qtz-feldspar-gneiss	Granitic leucosome			
STR3r	Grt-Pl-granulite	Graywacke			
STR3l	Qtz-Pl-granulite	Trondhjemitic leucosome	Granulite	Val Strona 1 km west of Forno, block from northern road side	44200/87750 (I)
RIM1p	Kfs-Grt-granulite	Pelite	Granulite	Boulder2 km S of Rimella, in river bed	
RIM1a	Kfs-Qtz-granulite	Arenite			
FIO1	Qtz-Grt-granulite	Pelite	Granulite	Val Fiorina 9 km north of Ornavasso, river bed 500 m SSE of In la Piana	676120/ 100600 (CH)
FIO2	Garnetite	Pelite?	Granulite	Same as sample FIO1	676120/ 100600 (CH)
FIO3	Grt-Hbl-metabasite	Gabbro	Granulite	Same as sample FIO1	676120/ 100600 (CH)
FIO4	Metasomatized peridotite	Peridotite	Granulite	River bed 500 m SSW of sample FIO1	675820/ 100110 (CH)
ISO4	Qtz-Kfs-Pl-granulite with Opx	Intermediate igneous rock, tuffite?	Granulite	Val Sesia 300 m SSE of Isola, bridge over Cavala River	35710/74945 (I)

Table 3 Modal analyses

	STR1r	STR1l	STR2r	STR2l	STR3r	STR3l	RIM1p	RIM1a	FIO1	FIO2	FIO3	FIO4	ISO4
Qtz	20	30	1	25	<1	48	2	64	35	0	0	0	15
Kfs	0	0	<1	50	<1	1	25	20	<1	0	0	0	25
Pl	5	60	20	20	50	48	<1	1	<1	5	20	0	30
Bt	50	6	40	1	9	<1	<1	<1	0	<1	0	0	<1
Ms	3	<1	0	0	0	0	0	0	0	0	0	0	0
Grt	<1	<1	15	2	40	3	50	15	30	90	30	0	15
Sil	20	3	20	1	0	0	20	0	20	0	0	0	0
Hbl	0	0	0	0	0	0	0	0	0	0	45	0	0
Opx	0	0	0	0	0	0	0	0	0	0	0	18	11
Cpx	0	0	0	0	0	0	0	0	0	0	2	25	0
Ol	0	0	0	0	0	0	0	0	0	0	0	55	0
Zir	<1	<1	<1	<1	<1	<1	<1	<1	<1	<1	<1	<1	<1
Mon	<1	0	<1	0	<1	0	<1	<1	<1	0	0	0	0
Ap	0	0	0	0	0	0	0	0	0	0	2	0	1
Rt	0	0	<1	0	<1	<1	1	<1	<1	0	0	0	0
Ilm	0	0	<1	0	0	0	2	<1	<1	0	0	0	0
All	<1	<1	0	0	0	0	0	0	0	0	0	0	0
Spl	0	0	0	0	0	0	0	0	0	0	0	2	0
Graph	1	0	4	<1	0	0	<1	<1	5	0	0	0	0
Opa	<1	<1	<1	<1	<1	<1	<1	<1	<1	4	1	<1	3
Alt	<1	<1	<1	<1	1	<1	<1	<1	10	1	1	<1	<1

The remaining group of samples (FIO1–FIO4), taken from the banks of the Fiorina river, comes from one of the lowermost crustal levels of the IZ. This part of the IZ is dominated by mafic and ultramafic rocks of the Mafic Formation, but also contains intercalations of the metasedimentary rocks. The lithological association exposed in the Fiorina Valley is peculiar. It contains several meter thick layers of garnetite commonly found at the borders between metabasic and metapelitic rocks. The origin of the garnetites was the subject of a geochemical investigation by Rivalenti et al. (1997), who conclude that the garnetite formed by a magmatic mixing process when the lower crustal gabbroic intrusions became infiltrated by anatectic melt derived from the adjacent metapelites. The samples FIO1, FIO2 and FIO3 represent a metapelite, a garnetite and a metagabbro, respectively, from one of the two ca. 10 m wide profiles that were investigated by Rivalenti et al. (1997). Their samples VO106, VO107 and

VO110 are similar or identical to samples FIO1, FIO2 and FIO3 of the present study. Sample FIO4, taken at the Fiorina river ca. 500 m SSW of the garnetite sample, originates from a peridotite layer of 2.5 m thickness which, where bordering upon a 30 cm thick calcsilicate layer, is calcite bearing over a width of 60 cm.

Analytical techniques

Zircon grains were mounted, ground and polished in 25 mm epoxy discs. The internal zoning pattern of near central crystal sections was revealed by a cathodoluminescence (CL) detection system at the ETH Zürich based on a scanning electron microscope (CamScan CS4), operating at a 13 kV accelerating potential.

The same sample mounts were later used for microanalytical U-Th-Pb analyses using the sensitive high-resolution ion-microprobe (SHRIMP II) at the Australian National University in Canberra. Detailed analytical procedures have been given in several earlier reports (e.g. Compston et al. 1992; Vavra et al. 1996). The spot size of the ion beam was between 15 and 25 μm. Sixteen analyses of the standard SL13 (age 572 Ma) were made during each of 6 analytical sessions and the analytical uncertainty in the reproducibility of the U-Pb age of the standard was between 1.5 and 2.8% (1σ). The errors calculated for the U-Pb ages of individual unknown samples (1σ in Table 4 and 2σ in Figs. 4, 5) are based on counting precision only and do not comprise the additional component of uncertainty given by the error of the calibration line. Although counting errors underestimate the total uncertainty of the absolute ages, they are considered as a criterion to check whether U-Pb ages from groups of unknown samples agree to within their individual errors and, thus, can be claimed to represent a single age. In the report of absolute U-Pb ages (Table 5), the uncertainty of the calibration line has been incorporated in the error calculation. The ^{208}Pb-based and ^{207}Pb-based methods of common Pb correction were applied without detectable differences in most results.

The uncertainty in the concentration measurements of Th and U is at least 15%, according to the total range of U concentrations measured in the standard. During the present SHRIMP work, the uniformity of the SL 13 standard zircon was about 2% (1σ), according to replicate U contents per analytical session, and this error allows for realistic comparisons of U concentration data from unknown samples. The Th/U ratios are determined independently from concentration measurements and have a better precision (less than 1%).

Secondary electron (SE) micrographs of crystal surfaces (Fig. 2: 32, 33) and energy-dispersive X-ray (EDX) analyses, for identification of inclusions in zircon crystals, were made on a scanning electron microscope (Cambridge Steroscan 250) at the University of Tübingen, using a 20 kV accelerating potential.

Morphology and internal structure of the zircons

Zircons from metasedimentary rocks and associated leucosomes

Zircons from the restite and leucosome portions of the anatectic quartzo-feldspathic metasediments of Val Strona (STR1, STR2 and STR3) have been separately investigated and their different characteristics are presented in turn.

Zircons from the restites (STR1r, STR2r, STR3r) contain inherited (detrital) cores with highly variable sizes. In some crystal sections, the cores are not revealed, probably due to their very small size. Many cores have an angular and fractured shape (Fig. 2: 7, 8). The primary growth zoning is well preserved in part of the cores (Fig. 2: 8), whereas in others it is largely obliterated and apparently replaced by strongly luminescent and nearly homogeneous zircon (denoted as high-CL in Fig. 2: 1).

The overgrowth on the cores has a volume largely exceeding that of the cores themselves. The morphology and internal structure of the overgrowth varies from sample to sample. In the amphibolite facies sample STR1r, the {110}-prism faces were completely blocked during overgrowth of the cores (Fig. 2: 1). The resulting habit became prismatic, partly with high elongations. The very low luminescence hardly reveals any internal structures. This particular type of overgrowth is also present as an incipient and volumetrically very small stage of overgrowth on most of the detrital cores of the higher grade (granulite facies) metasediments (Fig. 2: 7, 8, 12, 13, 14, 15, 17, 18, 19, 20), where it is too small to be analyzed. Secondary electron micrographs and EDX analyses show that the prismatic overgrowth is rich in inclusions and half-inclusions of sillimanite needles, indicating a metamorphic (anatectic) origin. The habit of zircon overgrowth in the transitional facies metapelite STR2r is stubby (short prismatic). The internal growth structure (Fig. 2: 3–5) is characterized by fir-tree sector zoning, a zoning pattern resulting from unsteady growth rates of numerous and small crystal faces (Vavra et al. 1996). This overgrowth is again rich in sillimanite needles (Fig. 2: 4, 5), as verified by EDX analyses. The SE micrograph (Fig. 2: 32) shows growth inhibitions by sillimanite needles at the surface of a zircon crystal. High-luminescence domains that are patchily distributed over the crystal (denoted as ZCA in Fig. 2: 3–5) nucleated (started) on sector boundaries and inclusions and partly overprint the original growth and sector zoning. In the granulite facies sample STR3r, two morphologically different stages of overgrowth on detrital cores can be distinguished (Fig. 2: 7, 8). The first stage has a prismatic habit with well preserved oscillatory growth zoning. The second stage is isometric with strong CL and only faint relics of primary structures (Fig. 2: 8). The zircon overgrowths in this sample and in all the other samples with higher metamorphic grades are poor in inclusions.

In zircons from the anatectic leucosomes in the granulite samples STR2l and STR3l (Fig. 2: 6 and 9), inherited cores have not been observed. The habit of these zircons is more prismatic and their primary zoning is altogether better preserved than in the stubby and isometric zircon overgrowths in the associated restites. In the amphibolite facies sample STR1, zircons from restitic and leucosome portions (Fig. 2: 1, 2) are not well distinguished. All zircons contain inherited cores, but many zircons in the leucosome present a final growth stage with oscillatory zoning at the tips of crystals (Fig. 2: 2).

While samples STR1, STR2 and STR3 indicate that zircon growth varies with metamorphic grade (upper

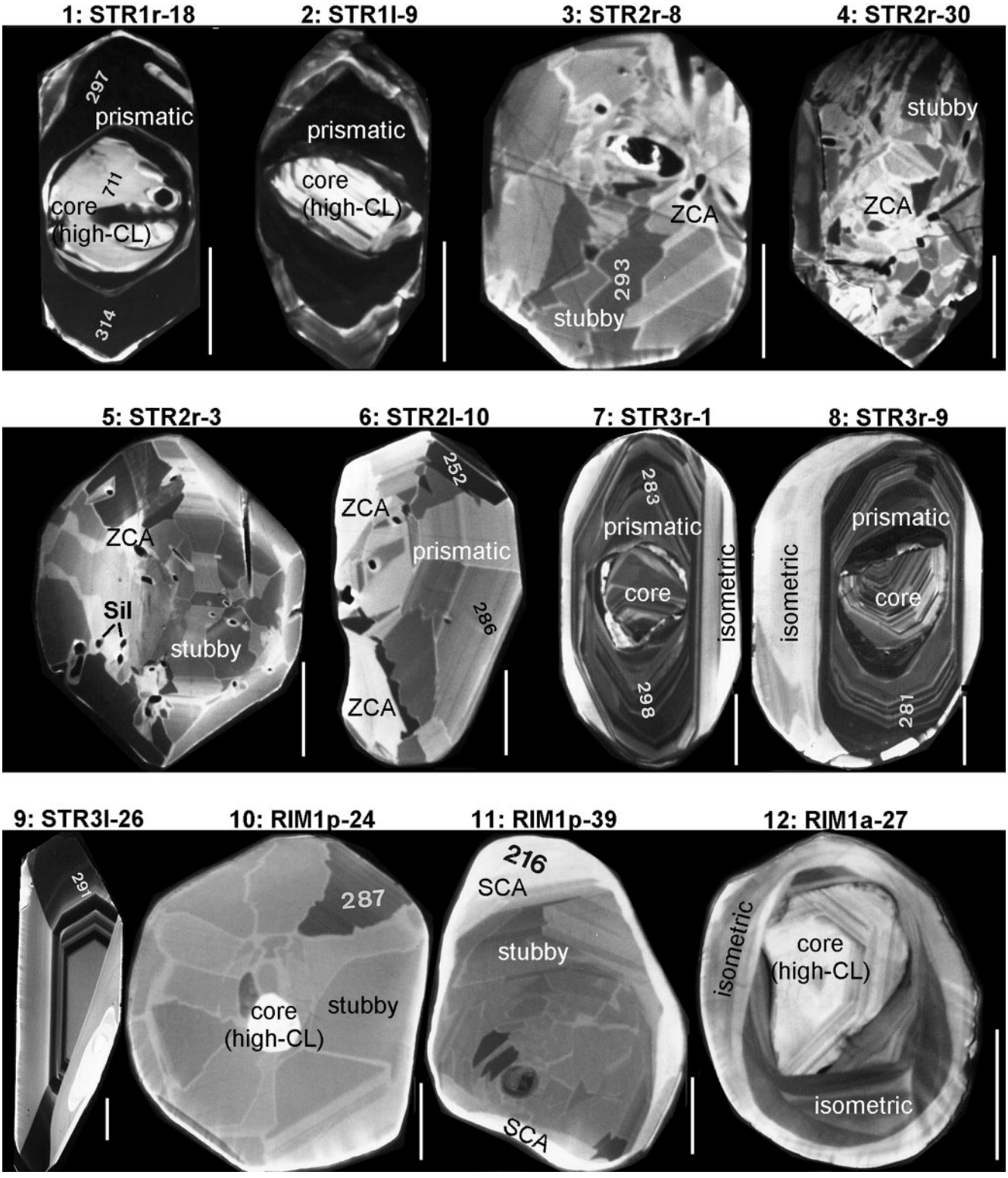

Fig. 2 1–31 Cathodoluminescence images of sections through zircon crystals. *Numbers within crystals* denote analytically concordant $^{206}Pb/^{238}U$ ages in Ma. Errors are given in Table 4. Scale *bars* are 30 μm. (*ZCA* zoning-controlled alteration, *SCA* surface-controlled alteration, *Sil* sillimanite). For explanation see text

amphibolite facies to granulite facies) and anatectic environment (restite and leucosome), the banded metapelite/meta-arenite sample RIM1 shows that growth characteristics also depend on lithology. The zircon overgrowth in the metapelite layer (RIM1p) is stubby with internal fir-tree zoning (Fig. 2: 10, 11), similar to

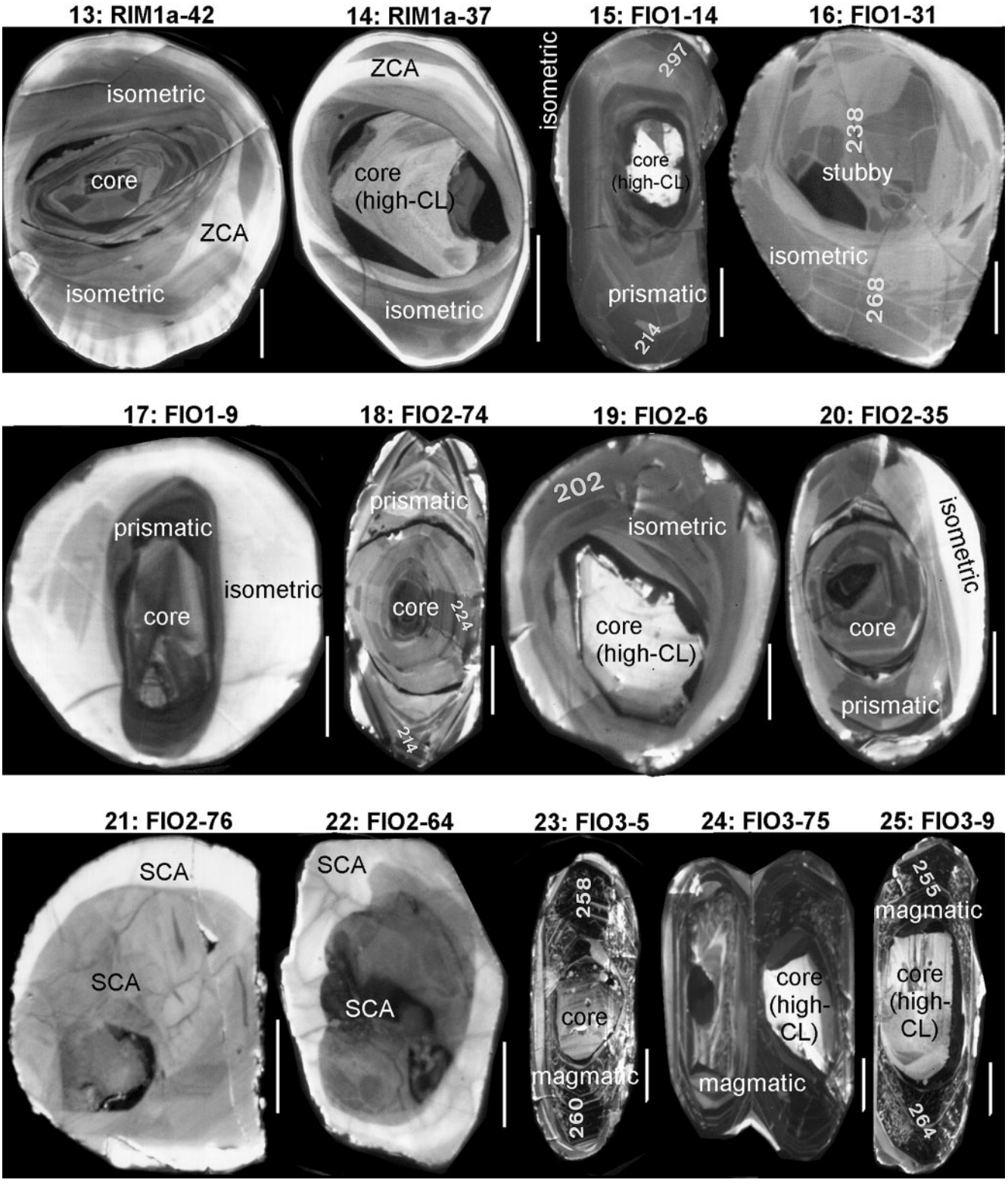

Fig. 2 (contd.)

zircons in metapelite sample STR2r, but the zircon overgrowth in the meta-arenite layer (RIM1a) is perfectly isometric with internal growth structures consisting of rounded shells (Fig. 2: 12–14). Some crystals of sample RIM1p are strongly corroded with rough crystal surfaces observed in SE images (not shown). The CL images of corroded crystals (e.g. Fig. 2: 11) reveal high-luminescence crystal rims (denoted as SCA) that truncate primary growth structures. The crystals of the meta-arenitic sample, on the other hand, are smoothly

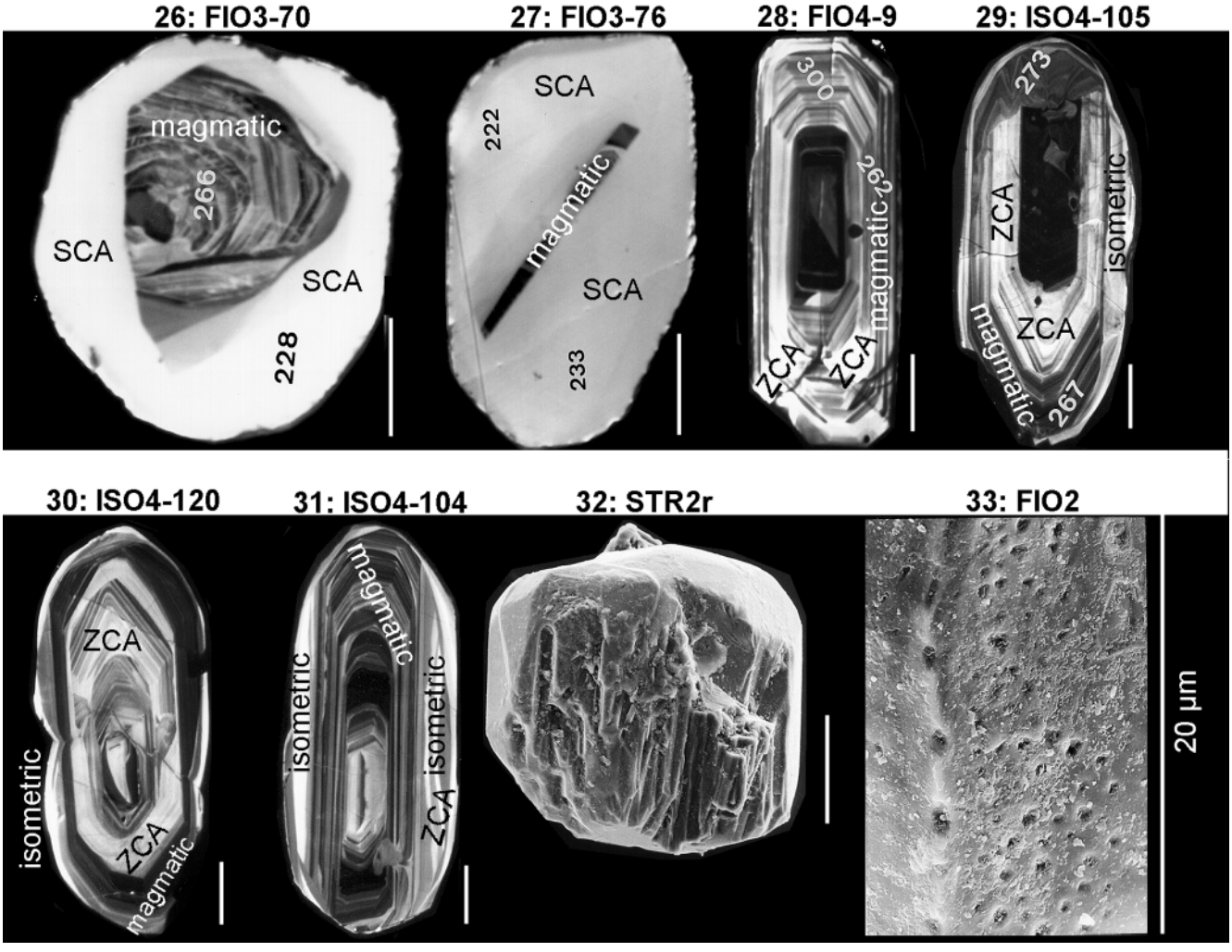

Fig. 2 (contd.)

rounded and uncorroded. High-luminescence domains occur at crystal rims as well as in the interior (denoted as ZCA in Fig. 2: 13, 14), their outline being guided by the primary isometric growth zoning.

The zircons from the granulite facies metapelite FIO1 of Val Fiorina resemble the zircons from the granulite facies metagreywacke STR3r of Val Strona, but the isometric type of overgrowth is volumetrically more important than prismatic and stubby overgrowth. In crystals where several types of overgrowths are observed, the isometric overgrowth follows prismatic or stubby overgrowth (Fig. 2: 15–16, 17), like in sample STR3r. Most of the isometric overgrowth is again highly luminescent and shows only faint relics of primary zoning. The prismatic and stubby types of overgrowth do not contain high-luminescence domains, but their internal structure is altogether fainter than observed in STR3r and other samples from the Val Strona area.

Despite its supposed magmatic origin (Rivalenti et al. 1997), the garnetite (FIO2) of the Val Fiorina profile contains zircons (Fig. 2: 18–20) showing much the same structural and morphological characteristics as the zircons in the adjacent metapelite (FIO1). The only notable difference is the higher degree of surface corrosion of the zircons in sample FIO2. Corrosion pits are concentrated on crystal edges, as shown by the SE micrograph (Fig. 2: 33). In heavily corroded crystals the primary growth structures are completely destroyed (denoted as SCA in Fig. 2: 21, 22). The alteration consists of highly-luminescent crystal rims below the corroded surfaces and channel structures or faintly patchy patterns in the crystal interiors.

Zircons from meta-igneous rocks

The zircons in the metagabbro (FIO3) are well distinguished from those in the metapelite and garnetite samples (FIO1 and FIO2). Their habit is prismatic and the internal growth zoning is euhedral (Fig. 2: 23–25), but barely visible due to rather low luminescence. Some of the crystals are heavily corroded and altered (denoted as SCA in Fig. 2: 26, 27), showing much the same type of alteration of crystal rims that is also found in the adjacent garnetite (Fig. 2: 21, 22). The

zircons of the peridotite (FIO4) also have a euhedral prismatic, thus typically magmatic, shape (Fig. 2: 28). They are distinguished from the metagabbro zircons by the absence of surface corrosion and alteration of crystal rims. High-luminescence domains (denoted as ZCA) are distributed over the crystals and are guided by the primary growth structure. Inherited cores are present in the metagabbro, but not in the metaperidotite zircons.

The meta-igneous granulite ISO4 contains a zircon population that is largely magmatic, but contaminated by a sedimentary component (Vavra et al. 1996). The magmatic zircons with prismatic internal zoning (Fig. 2: 29–31; and Fig. 2: 13 in Vavra et al. 1996) are covered by a small amount of isometric overgrowth. Its growth structure consists of roundish shells (denoted as isometric in Fig. 2: 29–31), very similar to the shell-type (isometric) overgrowth found in the meta-arenite sample RIM1a (Fig. 2: 12–14). High-luminescence domains (denoted as ZCA) occur in the magmatic crystals as well as in the isometric overgrowths and, in both cases, their outlines are guided by the primary growth and sector zoning.

Typology of alteration patterns

Most of the investigated crystals (Fig. 2) show domains where the cathodoluminescence (CL) is very strong. In some crystals, it is evident that strongly luminescent domains result from alteration of primary growth structures (growth banding and sector zoning). This is evident where the high-CL domains start (nucleate) on inclusions and sector boundaries (e.g. Fig. 2: 4, 5) and where they truncate the primary zoning (e.g. Fig. 2: 26). It is probable that all strongly luminescent crystal domains result from alteration processes. Two types of alteration pattern can tentatively be distinguished and will be substantiated by U-Th-Pb analyses. The first pattern is principally controlled and guided by primary structures like inclusions, sector boundaries and growth banding and appears to be unrelated to corrosion at crystal surfaces. This pattern will be called *zoning-controlled alteration* (ZCA; Fig. 2: 3–6, 13, 14, 28–31). The ZCA domains can easily be discerned within generations of stubby and prismatic growth (Fig. 2: 3–6, 28–30), but are rarely discerned within generations of isometric growth (Fig. 2: 13, 14, 31), because most of the isometric growth is strongly luminescent altogether (Fig. 2: 7, 8, 17, 20). Part of the inherited zircon cores is also strongly luminescent (Fig. 2: 1, 2, 10, 12, 14, 15, 19, 24, 25; high-CL) and may have been affected by the same or a similar alteration mechanism. The second pattern of alteration is represented by strongly luminescent crystal rims below corroded crystal surfaces and appears to be unrelated to primary structures. This pattern will be called *surface-controlled alteration* (SCA; Fig. 2: 11, 21, 22, 26, 27). The borders of the SCA domains are partly sharp and partly gradual. The interior parts of some affected crystals are faintly patchy (Fig. 2: 22) or show a pattern of irregular channels (Fig. 2: 21).

Th-U chemistry of the zircons

The Th and U concentrations of crystal domains analyzed by SHRIMP are shown in Fig. 3. It is observed that all the analyses from magmatic domains in the meta-igneous zircons (FIO3, FIO4, ISO4) have a rather constant Th/U ratio of about 0.3 (Fig. 3; triangles). The Th/U ratios of the metamorphic (anatectic) growths and overgrowths (in metasediments and leucosomes) are also fairly constant as long as only one single type of growth in a single sample is considered, but between different types of growth and between different samples the ratios are very different, spanning a range of 2 orders of magnitude (Fig. 3; squares, diamonds and circles).

On the one hand, there is an apparent correlation of the Th/U ratio and metamorphic grade, as suggested by the sequence of samples STR1, STR2 and STR3. On the other hand, the Th/U ratio also varies between the morphologically different types of growth within single samples. In the isometric type of growth (Fig. 3: circles) the Th/U ratio is by one order of magnitude higher than in the prismatic or stubby type of overgrowth (Fig. 3: squares). This is observed in samples STR3, FIO1 and FIO2 where prismatic (and stubby) overgrowth is followed by isometric overgrowth in single crystals, and also in sample RIM1 where stubby overgrowth occurs in the pelitic (RIM1p) and isometric overgrowth in the arenitic (RIM1a) lithology.

The strongly luminescent alteration domains (ZCA and SCA) are characterized by depletions of Th and U. In ZCA domains (Fig. 2: 3–6, 29, 30), the Th/U ratio is rather constant and has remained the same as in the adjacent unaltered domains (Fig. 3: STR2, STR3, ISO4; unfilled squares, diamonds and triangles). In the SCA domains of samples RIM1 and FIO2 (Fig. 2: 11, 21, 22), Th became more strongly depleted than U (Fig. 3: RIM1, FIO2; star symbols).

Radiometric U-Pb data of the zircons

The microanalytical $^{206}Pb/^{238}U$ and $^{207}Pb/^{235}U$ data and the calculated apparent ages are presented in Table 4. Data from the inherited zircon cores, in metasedimentary rocks and in metagabbro FIO3, are plotted in the concordia diagram of Fig. 4. It is observed that part of the inherited cores are analytically discordant. However, all the strongly luminescent cores (e.g. Fig. 2: 1) are analytically concordant.

The analyses from the metamorphic (anatectic) growth generations in the restitic metasediments and leucosomes and from the magmatic growth in the meta-igneous rocks are not plotted in the concordia diagram, because all of them are analytically concordant. Since

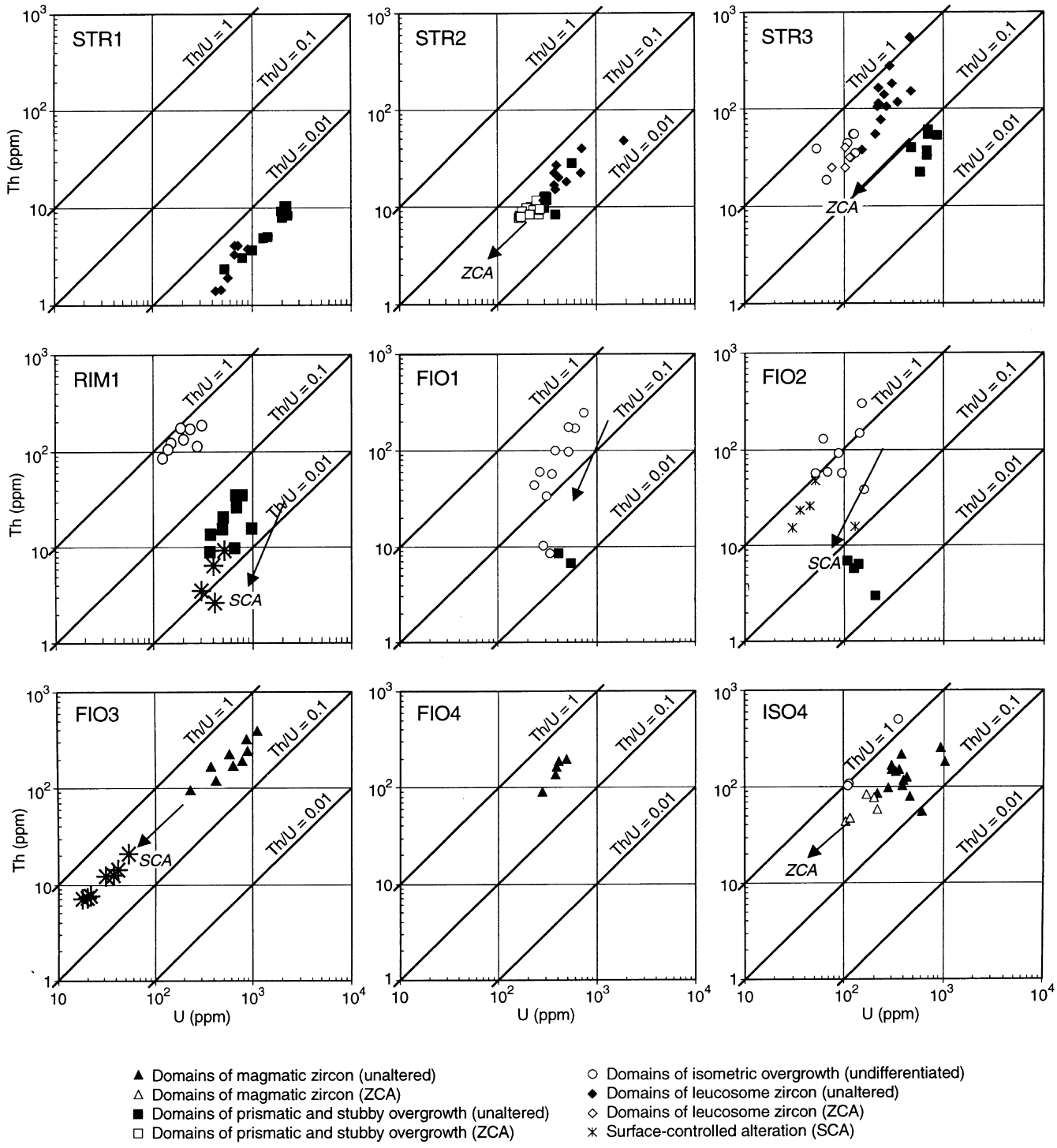

Fig. 3 Th and U concentrations of zircon domains analyzed by SHRIMP. *Arrows* indicate depletion by zoning-controlled alteration (*ZCA*) and surface-controlled alteration (*SCA*)

the $^{207}Pb/^{238}U$ data are less precise than the $^{206}Pb/^{238}U$ data and do not provide any additional age constraints, only the apparent $^{206}Pb/^{238}U$ ages are relevant to the discrimination of age components. The apparent ages are presented in the diagrams of Fig. 5. Within single rock samples, the apparent ages scatter largely in excess of their analytical uncertainty, thus, the U-Pb system of zircons became complex by one or several of the following mechanisms: multiple growth of new zircon, multiple Pb-loss events, partial Pb-loss.

The recognition and geological interpretation of age components within inherited cores, metamorphic (anatectic) overgrowths and magmatic zircons is the subject of the following discussion.

Table 4 U-Th-Pb microanalyses of zircon Errors are 1σ

Grain spot	Type[a]	f[b] %	Ratios corrected for common Pb:		Apparent ages (Ma):		Th (ppm)	U (ppm)
			$\frac{^{206}Pb^{c}}{^{238}U}$	$\frac{^{207}Pb^{d}}{^{235}U}$	$\frac{^{206}Pb^{c}}{^{238}U}$	$\frac{^{207}Pb^{d}}{^{235}U}$		
Metasedimentary granulites and associated Leucosomes								
STR1r-1.2	Prism	0.1	0.04920 ± 0.00035	0.3549 ± 0.0054	310 ± 2	308 ± 4	4	1008
STR1r-2.1	Prism	0.1	0.04358 ± 0.00023	0.3119 ± 0.0035	275 ± 1	276 ± 3	8	2149
STR1r-2.2	Prism	1.5	0.04885 ± 0.00032	0.3487 ± 0.0061	307 ± 2	304 ± 5	5	1428
STR1r-13.1	Prism	0.0	0.04162 ± 0.00029	0.2854 ± 0.0048	263 ± 2	255 ± 4	10	2243
STR1r-18.1	Prism	0.0	0.04710 ± 0.00026	0.3337 ± 0.0042	297 ± 2	292 ± 3	11	2154
STR1r-18.2	Core br	0.3	0.11662 ± 0.00148	1.0165 ± 0.0268	711 ± 9	712 ± 14	45	273
STR1r-18.3	Prism	0.0	0.04991 ± 0.00027	0.3540 ± 0.0042	314 ± 2	308 ± 3	9	1961
STR1r-19.1	Prism	0.2	0.04349 ± 0.00029	0.3112 ± 0.0049	274 ± 2	275 ± 4	10	2141
STR1r-20.1	Prism	0.1	0.04897 ± 0.00026	0.3464 ± 0.0042	308 ± 2	302 ± 3	8	2022
STR1r-20.2	Prism	0.1	0.04488 ± 0.00024	0.3251 ± 0.0040	283 ± 1	286 ± 3	8	2279
STR1r-21.1	Prism	0.5	0.04928 ± 0.00055	0.3477 ± 0.0098	310 ± 3	303 ± 7	2	527
STR1r-26.1	Prism	0.5	0.04955 ± 0.00043	0.3680 ± 0.0072	312 ± 3	318 ± 5	3	793
STR1r-32.1	Prism	0.2	0.04849 ± 0.00032	0.3408 ± 0.0051	305 ± 2	298 ± 4	10	2119
STR1r-32.2	Prism	0.2	0.04773 ± 0.00032	0.3346 ± 0.0052	301 ± 2	293 ± 4	11	2257
STR1r-33.2	Prism	0.0	0.04687 ± 0.00032	0.3250 ± 0.0050	295 ± 2	286 ± 4	5	1289
STR1l-1.1	Leuc	0.2	0.04703 ± 0.00045	0.3273 ± 0.0074	296 ± 3	288 ± 6	4	721
STR1l-2.2	Leuc	0.3	0.04573 ± 0.00046	0.3226 ± 0.0076	288 ± 3	284 ± 6	4	676
STR1l-6.1	Leuc	0.3	0.04666 ± 0.00043	0.3346 ± 0.0070	294 ± 3	293 ± 5	4	905
STR1l-23.1	Core br	2.2	0.08716 ± 0.00238	0.6990 ± 0.0586	539 ± 14	538 ± 35	15	71
STR1l-26.2	Leuc	0.3	0.04750 ± 0.00049	0.3358 ± 0.0085	299 ± 3	294 ± 6	2	579
STR1l-29.1	Leuc	0.3	0.04728 ± 0.00052	0.3215 ± 0.0093	298 ± 3	283 ± 7	1	487
STR1l-33.1	Leuc	0.2	0.04732 ± 0.00056	0.3420 ± 0.0089	298 ± 3	299 ± 7	3	660
STR1l-36.1	Leuc	1.0	0.04766 ± 0.00056	0.3627 ± 0.0101	300 ± 3	314 ± 8	1	427
STR2r-6.2	Stub	0.8	0.04713 ± 0.00045	0.3331 ± 0.0085	297 ± 3	292 ± 6	10	216
STR2r-8.1	Stub	0.5	0.04652 ± 0.00077	0.3277 ± 0.0151	293 ± 5	288 ± 12	13	302
STR2r-10.1	Stub ZCA	1.9	0.04126 ± 0.00098	0.2790 ± 0.0234	261 ± 6	250 ± 19	9	176
STR2r-11.2	Stub	0.1	0.04559 ± 0.00040	0.3165 ± 0.0066	287 ± 2	279 ± 05	10	297
STR2r-12.1	Stub	0.9	0.04520 ± 0.00073	0.3374 ± 0.0137	285 ± 5	295 ± 10	11	300
STR2r-12.2	Stub	3.9	0.04375 ± 0.00068	0.2978 ± 0.0184	276 ± 4	265 ± 14	13	309
STR2r-20.1	Stub ZCA	2.2	0.03874 ± 0.00094	0.3166 ± 0.0218	245 ± 6	279 ± 17	8	174
STR2r-21.1	Stub ZCA	1.6	0.04222 ± 0.00066	0.3381 ± 0.0137	267 ± 4	296 ± 10	10	242
STR2r-21.2	Stub ZCA	1.0	0.03938 ± 0.00060	0.2804 ± 0.0125	249 ± 4	251 ± 10	12	247
STR2r-21.3	Stub ZCA	1.9	0.04475 ± 0.00096	0.3503 ± 0.0211	282 ± 6	305 ± 16	8	165
STR2r-21.4	Stub ZCA	1.3	0.04296 ± 0.00089	0.3124 ± 0.0188	271 ± 5	276 ± 15	10	198
STR2r-26.1	Stub	0.2	0.04645 ± 0.00061	0.3294 ± 0.0106	293 ± 4	289 ± 08	29	566
STR2r-26.1	Stub ZCA	1.4	0.04424 ± 0.00075	0.2769 ± 0.0164	279 ± 5	248 ± 13	9	200
STR2r-26.2	Stub ZCA	0.7	0.03929 ± 0.00079	0.2613 ± 0.0162	248 ± 5	236 ± 13	9	227
STR2r-27.1	Stub ZCA	1.4	0.04585 ± 0.00090	0.3175 ± 0.0188	289 ± 6	280 ± 14	10	247
STR2r-32.1	Stub ZCA	1.7	0.04150 ± 0.00081	0.2830 ± 0.0185	262 ± 5	253 ± 15	8	167
STR2r-34.1	Stub ZCA	1.2	0.03872 ± 0.00071	0.2691 ± 0.0157	245 ± 4	242 ± 13	8	212
STR2r-34.2	Stub	0.4	0.04589 ± 0.00078	0.3207 ± 0.0141	289 ± 5	282 ± 11	13	299
STR2r-35.1	Stub	0.6	0.03988 ± 0.00057	0.2802 ± 0.0108	252 ± 4	251 ± 9	8	384
STR2r-44.1	Core br	4.9	0.10736 ± 0.00695	0.6458 ± 0.2089	657 ± 40	506 ± 129	10	18
STR2r-57.1	Stub ZCA	2.3	0.04001 ± 0.00072	0.3068 ± 0.0167	253 ± 4	272 ± 13	9	253
STR2r-61.1	Stub ZCA	1.2	0.04329 ± 0.00088	0.2965 ± 0.0178	273 ± 5	264 ± 14	9	237
STR2r-65.2	Stub ZCA	3.8	0.04312 ± 0.00087	0.3037 ± 0.0231	272 ± 5	269 ± 18	9	260
STR2r-66.1	Stub	0.6	0.04576 ± 0.00076	0.3278 ± 0.0149	288 ± 5	288 ± 11	12	308
STR2r-66.2	Stub ZCA	0.5	0.03923 ± 0.00070	0.2722 ± 0.0135	248 ± 4	244 ± 11	10	268
STR2r-71.1	Core	0.7	0.08917 ± 0.00110	0.8133 ± 0.0391	551 ± 7	604 ± 22	441	484
STR2r-74.1	Core	0.9	0.06265 ± 0.00120	0.4137 ± 0.0290	392 ± 7	352 ± 21	73	228
STR2r-74.2	Core	1.3	0.05388 ± 0.00092	0.4013 ± 0.0248	338 ± 6	343 ± 18	113	322
STR2l-1.1	Leuc	0.1	0.04352 ± 0.00033	0.3103 ± 0.0061	275 ± 2	274 ± 5	40	718
STR2l-1.3	Leuc	0.1	0.04566 ± 0.00034	0.3238 ± 0.0057	288 ± 2	285 ± 4	18	501
STR2l-4.1	Leuc	0.0	0.04359 ± 0.00029	0.3073 ± 0.0052	275 ± 2	272 ± 4	20	416
STR2l-9.1	Leuc	0.3	0.04166 ± 0.00030	0.2977 ± 0.0053	263 ± 2	265 ± 4	22	699
STR2l-10.1	Leuc	0.1	0.04533 ± 0.00045	0.3189 ± 0.0079	286 ± 3	281 ± 6	12	291
STR2l-10.4	Leuc	0.3	0.03990 ± 0.00032	0.2832 ± 0.0059	252 ± 2	253 ± 5	27	393
STR2l-12.1	Leuc	0.3	0.04636 ± 0.00039	0.3377 ± 0.0073	292 ± 2	295 ± 6	15	388
STR2l-12.2	Leuc	0.0	0.04708 ± 0.00040	0.3286 ± 0.0071	297 ± 2	289 ± 5	17	377
STR2l-48.1	Leuc	0.1	0.04010 ± 0.00029	0.2825 ± 0.0049	253 ± 2	253 ± 4	48	1900
STR2l-48.2	Leuc	0.7	0.04594 ± 0.00070	0.3064 ± 0.0137	290 ± 4	271 ± 11	23	370
STR3r-1.1	Prism	0.3	0.04736 ± 0.00049	0.3283 ± 0.0092	298 ± 3	288 ± 7	37	675
STR3r-1.2	Prism	0.3	0.04489 ± 0.00042	0.3220 ± 0.0078	283 ± 3	283 ± 6	22	579
STR3r-2.2	Prism	0.9	0.04222 ± 0.00043	0.3098 ± 0.0085	267 ± 3	274 ± 7	33	674

Table 4 (contd.)

Grain spot	Type[a]	f[b] %	Ratios corrected for common Pb:		Apparent ages (Ma):		Th (ppm)	U (ppm)
			$^{206}Pb^{c}/^{238}U$	$^{207}Pb^{d}/^{235}U$	$^{206}Pb^{c}/^{238}U$	$^{207}Pb^{d}/^{235}U$		
STR3r-9.3	Prism	0.8	0.04452 ± 0.00039	0.3268 ± 0.0081	281 ± 2	287 ± 6	54	690
STR3r-9.4	Core	0.3	0.09998 ± 0.00108	0.9043 ± 0.0253	614 ± 6	654 ± 14	167	435
STR3r-9.5	Isom	2.0	0.04635 ± 0.00093	0.3587 ± 0.0289	292 ± 6	311 ± 22	55	125
STR3r-16.1	Prism	0.1	0.04565 ± 0.00039	0.3230 ± 0.0073	288 ± 2	284 ± 6	53	844
STR3r-18.1	Isom	1.2	0.04193 ± 0.00064	0.2645 ± 0.0194	265 ± 4	238 ± 16	54	127
STR3r-18.3	Isom	4.2	0.04274 ± 0.00071	0.2674 ± 0.0250	270 ± 4	241 ± 20	44	108
STR3r-32.1	Isom	1.8	0.04433 ± 0.00098	0.2920 ± 0.0287	280 ± 6	260 ± 23	19	67
STR3r-32.2	Isom	2.6	0.03884 ± 0.00100	0.2990 ± 0.0421	246 ± 6	266 ± 33	39	53
STR3r-48.1	Prism	0.2	0.04762 ± 0.00034	0.3480 ± 0.0062	300 ± 2	303 ± 5	40	468
STR3r-48.2	Prism	0.1	0.04846 ± 0.00028	0.3551 ± 0.0050	305 ± 2	309 ± 4	60	699
STR3r-53.1	Isom	0.5	0.04219 ± 0.00054	0.2932 ± 0.0133	266 ± 3	261 ± 10	35	131
STR3l-1.1	Leuc	0.2	0.04726 ± 0.00041	0.3651 ± 0.0225	298 ± 3	316 ± 17	542	458
STR3l-1.2	Leuc	0.5	0.04292 ± 0.00033	0.2825 ± 0.0147	271 ± 2	253 ± 12	281	292
STR3l-5.1	Leuc ZCA	1.6	0.04051 ± 0.00071	0.2772 ± 0.0190	256 ± 4	248 ± 15	25	104
STR3l-5.2	Leuc	0.6	0.04704 ± 0.00054	0.3303 ± 0.0164	296 ± 3	290 ± 13	113	224
STR3l-8.1	Leuc	1.7	0.04631 ± 0.00085	0.3784 ± 0.0326	292 ± 5	326 ± 24	166	224
STR3l-8.1	Leuc ZCA	3.6	0.04596 ± 0.00076	0.3269 ± 0.0245	290 ± 5	287 ± 19	25	77
STR3l-11.2	Leuc	0.4	0.04771 ± 0.00054	0.3652 ± 0.0147	300 ± 3	316 ± 11	55	208
STR3l-17.1	Leuc	1.0	0.04517 ± 0.00067	0.3235 ± 0.0169	285 ± 4	285 ± 13	38	153
STR3l-25.1	Leuc	0.2	0.04561 ± 0.00036	0.3317 ± 0.0114	287 ± 2	291 ± 9	181	303
STR3l-25.2	Leuc	0.0	0.04493 ± 0.00029	0.3143 ± 0.0071	283 ± 2	277 ± 5	153	467
STR3l-25.3	Leuc ZCA	1.3	0.04257 ± 0.00071	0.2806 ± 0.0204	269 ± 4	251 ± 16	40	102
STR3l-26.1	Leuc	0.8	0.04619 ± 0.00051	0.3385 ± 0.0139	291 ± 3	296 ± 11	104	267
STR3l-29.1	Leuc ZCA	1.1	0.04418 ± 0.00056	0.3002 ± 0.0145	279 ± 3	267 ± 11	31	118
STR3l-30.2	Leuc	0.3	0.04595 ± 0.00036	0.3431 ± 0.0094	290 ± 2	299 ± 7	116	350
STR3l-30.3	Leuc	0.2	0.04521 ± 0.00048	0.3149 ± 0.0131	285 ± 3	278 ± 10	76	238
STR3l-41.1	Leuc ZCA	1.4	0.04241 ± 0.00070	0.2771 ± 0.0190	268 ± 4	248 ± 15	31	114
STR3l-41.2	Leuc	1.7	0.04799 ± 0.00081	0.3668 ± 0.0289	302 ± 5	317 ± 21	141	255
STR3l-41.3	Leuc	1.3	0.04575 ± 0.00083	0.3409 ± 0.0281	288 ± 5	298 ± 21	107	215
RIM1p-22.1	Stub	0.0	0.04362 ± 0.00039	0.2906 ± 0.0052	275 ± 2	259 ± 4	18	921
RIM1p-22.2	Stub	0.8	0.04401 ± 0.00048	0.3220 ± 0.0077	278 ± 3	283 ± 6	22	469
RIM1p-24.1	Stub	0.0	0.04545 ± 0.00046	0.3240 ± 0.0067	287 ± 3	285 ± 5	39	732
RIM1p-39.1	Stub SCA	1.5	0.03413 ± 0.00054	0.2687 ± 0.0093	216 ± 3	242 ± 7	4	290
RIM1p-96.1	Stub	0.1	0.04307 ± 0.00047	0.3015 ± 0.0069	272 ± 3	268 ± 5	39	666
RIM1p-106.1	Stub SCA	0.2	0.03546 ± 0.00044	0.2494 ± 0.0064	225 ± 3	226 ± 5	11	496
RIM1p-106.2	Stub	0.2	0.04378 ± 0.00066	0.3057 ± 0.0094	276 ± 4	271 ± 7	9	364
RIM1p-107.1	Stub SCA	0.4	0.03602 ± 0.00052	0.2572 ± 0.0077	228 ± 3	232 ± 6	8	373
RIM1p-107.2	Stub	0.0	0.04834 ± 0.00068	0.3370 ± 0.0092	304 ± 4	295 ± 7	15	369
RIM1p-108.1	Stub	0.2	0.04537 ± 0.00054	0.3289 ± 0.0076	286 ± 3	289 ± 6	10	607
RIM1p-119.1	Stub SCA	2.0	0.03484 ± 0.00078	0.2332 ± 0.0137	221 ± 5	213 ± 11	3	393
RIM1p-139.1	Stub	0.3	0.04403 ± 0.00057	0.3154 ± 0.0085	278 ± 4	278 ± 7	18	469
RIM1p-139.2	Stub	0.0	0.04670 ± 0.00056	0.3148 ± 0.0079	294 ± 3	278 ± 6	30	663
RIM1a-13.1	Isom	0.5	0.04058 ± 0.00078	0.2833 ± 0.0242	256 ± 5	253 ± 19	181	200
RIM1a-18.1	Isom	1.1	0.04127 ± 0.00092	0.3340 ± 0.0237	261 ± 6	293 ± 18	201	323
RIM1a-18.2	Isom	1.1	0.04394 ± 0.00151	0.3467 ± 0.0434	277 ± 9	302 ± 33	116	151
RIM1a-19.1	Isom	0.6	0.03946 ± 0.00073	0.3021 ± 0.0203	249 ± 5	268 ± 16	145	207
RIM1a-36.2	Isom	2.6	0.04296 ± 0.00146	0.2438 ± 0.0439	271 ± 9	222 ± 36	93	131
RIM1a-48.1	Isom	0.4	0.04115 ± 0.00086	0.2719 ± 0.0260	260 ± 5	244 ± 21	132	155
RIM1a-70.1	Core	1.1	0.07188 ± 0.00093	0.6750 ± 0.0195	447 ± 6	524 ± 12	198	404
RIM1a-75.1	Isom	1.2	0.04202 ± 0.00105	0.2743 ± 0.0233	265 ± 6	246 ± 19	125	289
RIM1a-75.2	Isom	1.3	0.04219 ± 0.00107	0.2954 ± 0.0311	266 ± 7	263 ± 24	183	245
FIO1-5.1	Core br	1.9	0.19170 ± 0.00301	2.1187 ± 0.0699	1131 ± 16	1155 ± 23	68	155
FIO1-11.1	Isom	1.4	0.04356 ± 0.00064	0.2484 ± 0.0175	275 ± 4	225 ± 14	45	232
FIO1-13.1	Isom	2.3	0.03670 ± 0.00071	0.3291 ± 0.0165	232 ± 4	289 ± 13	9	329
FIO1-14.1	Prism	1.9	0.03381 ± 0.00045	0.2419 ± 0.0105	214 ± 3	220 ± 9	7	543
FIO1-14.2	Prism	1.4	0.04716 ± 0.00051	0.3501 ± 0.0107	297 ± 3	305 ± 8	9	410
FIO1-15.1	Isom	1.6	0.03952 ± 0.00053	0.2739 ± 0.0143	250 ± 3	246 ± 11	58	348
FIO1-26.1	Isom	0.8	0.03646 ± 0.00045	0.2513 ± 0.0134	231 ± 3	228 ± 11	247	749
FIO1-26.2	Isom	1.5	0.03522 ± 0.00056	0.2250 ± 0.0187	223 ± 4	206 ± 16	175	520
FIO1-31.1	Isom	1.9	0.03775 ± 0.00046	0.2620 ± 0.0136	239 ± 3	236 ± 11	97	520
FIO1-31.2	Isom	1.6	0.04258 ± 0.00059	0.3799 ± 0.0166	269 ± 4	327 ± 12	170	598
FIO1-33.1	Isom	1.1	0.04665 ± 0.00052	0.3530 ± 0.0136	294 ± 3	307 ± 10	101	377
FIO1-33.2	Isom	2.7	0.04404 ± 0.00061	0.3198 ± 0.0183	278 ± 4	282 ± 14	61	261
FIO1-35.1	Isom	1.7	0.04635 ± 0.00074	0.2985 ± 0.0210	292 ± 5	265 ± 16	34	310
FIO1-35.2	Isom	2.6	0.03368 ± 0.00058	0.2406 ± 0.0152	214 ± 4	219 ± 12	10	282

Table 4 (contd.)

Grain spot	Type[a]	f[b] %	Ratios corrected for common Pb:		Apparent ages (Ma):		Th (ppm)	U (ppm)
			$\frac{^{206}Pb^{c}}{^{238}U}$	$\frac{^{207}Pb^{d}}{^{235}U}$	$\frac{^{206}Pb^{c}}{^{238}U}$	$\frac{^{207}Pb^{d}}{^{235}U}$		
FIO2-8.2	Prism	2.8	0.04091 ± 0.00064	0.2679 ± 0.0163	258 ± 4	241 ± 13	7	109
FIO2-10.1	SCA	8.0	0.03445 ± 0.00096	0.2322 ± 0.0431	218 ± 6	212 ± 35	15	30
FIO2-11.1	Prism	7.8	0.03769 ± 0.00052	0.3115 ± 0.0183	239 ± 3	275 ± 14	6	126
FIO2-11.2	Prism	1.4	0.04580 ± 0.00059	0.2935 ± 0.0125	289 ± 4	261 ± 10	6	140
FIO2-12.1	SCA	10.2	0.03415 ± 0.00087	0.2732 ± 0.0452	216 ± 5	245 ± 36	23	37
FIO2-45.1	Isom	8.5	0.03846 ± 0.00069	0.2196 ± 0.0373	243 ± 4	202 ± 31	58	69
FIO2-45.2	Isom	6.5	0.03525 ± 0.00059	0.2746 ± 0.0335	223 ± 4	246 ± 27	91	88
FIO2-52.1	Isom	3.9	0.03435 ± 0.00052	0.2342 ± 0.0212	218 ± 3	214 ± 17	57	95
FIO2-55.1	Isom	4.7	0.03514 ± 0.00044	0.2497 ± 0.0152	223 ± 3	226 ± 12	39	161
FIO2-56.1	Isom	12.5	0.03428 ± 0.00067	0.1272 ± 0.0607	217 ± 4	122 ± 55	130	62
FIO2-56.2	Isom	10.1	0.03915 ± 0.00078	0.1141 ± 0.0472	248 ± 5	110 ± 43	58	51
FIO2-62.1	SCA	12.3	0.03440 ± 0.00085	0.2012 ± 0.0466	218 ± 5	186 ± 39	26	46
FIO2-70.2	SCA	5.4	0.03496 ± 0.00079	0.2190 ± 0.0276	222 ± 5	201 ± 23	16	129
FIO2-74.1	Prism	4.1	0.03393 ± 0.00063	0.2454 ± 0.0182	215 ± 4	223 ± 15	3	206
FIO2-74.2	Core	3.1	0.03552 ± 0.00060	0.2248 ± 0.0203	225 ± 4	206 ± 17	101	338
FIO2-200.1	Isom	0.8	0.04707 ± 0.00095	0.3032 ± 0.0801	296 ± 6	269 ± 62	299	153
FIO2-200.2	SCA	1.7	0.03284 ± 0.00094	0.2108 ± 0.0444	208 ± 6	194 ± 37	48	51
Metagabbro								
FIO3-5.1	Mag	1.7	0.04126 ± 0.00024	0.3118 ± 0.0061	261 ± 1	276 ± 5	164	806
FIO3-5.2	Core	3.2	0.05870 ± 0.00054	0.5511 ± 0.0216	368 ± 3	446 ± 14	211	261
FIO3-5.3	Mag	0.4	0.04088 ± 0.00019	0.3011 ± 0.0042	258 ± 1	267 ± 3	206	1040
FIO3-9.1	Mag	0.6	0.04041 ± 0.00020	0.2856 ± 0.0048	255 ± 1	255 ± 4	175	930
FIO3-9.2	Mag	0.7	0.04192 ± 0.00025	0.2949 ± 0.0063	265 ± 2	262 ± 5	124	548
FIO3-9.3	Core br	1.6	0.05048 ± 0.00067	0.3832 ± 0.0354	317 ± 4	329 ± 26	121	92
FIO3-27.1	SCA	6.0	0.03812 ± 0.00119	0.2710 ± 0.0436	241 ± 7	244 ± 35	15	38
FIO3-28.1	SCA	14.6	0.03499 ± 0.00106	0.3532 ± 0.0564	222 ± 7	307 ± 42	14	34
FIO3-35.1	Mag	1.4	0.03862 ± 0.00025	0.2865 ± 0.0076	244 ± 2	256 ± 6	184	476
FIO3-35.2	Mag	0.6	0.03852 ± 0.00023	0.2685 ± 0.0061	244 ± 1	241 ± 5	218	748
FIO3-35.3	SCA	6.5	0.03117 ± 0.00063	0.2460 ± 0.0270	199 ± 5	223 ± 22	23	52
FIO3-36.1	Mag	0.1	0.04645 ± 0.00017	0.3287 ± 0.0039	293 ± 1	289 ± 3	348	1433
FIO3-36.2	Mag	0.6	0.04087 ± 0.00019	0.3028 ± 0.0050	258 ± 1	269 ± 4	282	1019
FIO3-39.1	SCA	10.9	0.03251 ± 0.00112	0.2295 ± 0.0557	206 ± 7	210 ± 46	8	19
FIO3-41.1	SCA	22.4	0.03632 ± 0.00126	0.2445 ± 0.0779	230 ± 8	222 ± 64	7	17
FIO3-41.2	SCA	19.8	0.03830 ± 0.00127	0.1437 ± 0.0737	242 ± 8	136 ± 65	8	18
FIO3-70.1	SCA	2.4	0.03612 ± 0.00093	0.2122 ± 0.0313	229 ± 6	195 ± 26	13	30
FIO3-70.2	Mag	1.3	0.04218 ± 0.00040	0.3097 ± 0.0110	266 ± 2	274 ± 9	91	297
FIO3-76.1	SCA	12.5	0.03744 ± 0.00117	0.2117 ± 0.0562	237 ± 7	195 ± 47	8	19
FIO3-76.2	SCA	18.9	0.03594 ± 0.00111	0.0438 ± 0.0623	228 ± 7	44 ± 61	8	20
Metaperidotite								
FIO4-1.1	Mag	6.0	0.04646 ± 0.00033	0.3110 ± 0.0117	293 ± 2	275 ± 9	137	378
FIO4-9.1	Mag	0.6	0.04764 ± 0.00041	0.3130 ± 0.0122	300 ± 3	277 ± 9	166	387
FIO4-9.2	Mag	1.3	0.04150 ± 0.00027	0.2842 ± 0.0086	262 ± 2	254 ± 7	199	494
FIO4-17.1	Mag	1.3	0.04637 ± 0.00031	0.3388 ± 0.0096	292 ± 2	296 ± 7	189	414
FIO4-17.2	Mag	6.7	0.04499 ± 0.00039	0.2620 ± 0.0149	284 ± 2	236 ± 12	91	277
Meta-igneous granulite								
ISO4-3.1	Mag	1.7	0.05002 ± 0.00087	0.3626 ± 0.0191	315 ± 5	314 ± 14	97	278
ISO4-11.1	Mag	0.4	0.05700 ± 0.00061	0.4161 ± 0.0129	357 ± 4	353 ± 9	153	363
ISO4-11.2	Mag ZCA	0.3	0.04738 ± 0.00096	0.3324 ± 0.0210	298 ± 6	291 ± 16	43	105
ISO4-15.1	Isom	0.1	0.04420 ± 0.00053	0.2909 ± 0.0231	279 ± 3	259 ± 18	495	346
ISO4-20.3	Isom	0.4	0.04642 ± 0.00095	0.2743 ± 0.0318	293 ± 6	246 ± 25	109	114
ISO4-20.4	Mag	0.2	0.05626 ± 0.00076	0.4128 ± 0.0169	353 ± 5	351 ± 12	152	302
ISO4-22.1	Mag ZCA	0.6	0.04449 ± 0.00073	0.3030 ± 0.0139	281 ± 4	269 ± 11	57	215
ISO4-22.2	Isom	0.9	0.04012 ± 0.00091	0.2593 ± 0.0299	254 ± 6	234 ± 24	103	111
ISO4-22.3	Mag ZCA	0.3	0.04352 ± 0.00085	0.3355 ± 0.0204	275 ± 5	294 ± 16	83	167
ISO4-22.4	Mag	0.0	0.05674 ± 0.00065	0.4156 ± 0.0114	356 ± 4	353 ± 8	126	429
ISO4-25.1	Mag	0.6	0.05468 ± 0.00075	0.4033 ± 0.0172	343 ± 5	344 ± 12	167	304
ISO4-26.1	Mag	0.0	0.05321 ± 0.00052	0.3470 ± 0.0078	334 ± 3	302 ± 6	79	461
ISO4-26.2	Mag ZCA	0.2	0.04788 ± 0.00071	0.3334 ± 0.0146	302 ± 4	292 ± 11	78	200
ISO4-42.1	Mag ZCA	3.8	0.04275 ± 0.00155	0.4186 ± 0.0419	270 ± 10	355 ± 30	47	115
ISO4-69.1	Mag	1.9	0.05144 ± 0.00108	0.3851 ± 0.0238	323 ± 7	331 ± 17	116	395
ISO4-69.2	Mag	0.0	0.05288 ± 0.00106	0.3758 ± 0.0186	332 ± 6	324 ± 14	104	389
ISO4-103.1	Mag	0.8	0.05572 ± 0.00123	0.4285 ± 0.0262	350 ± 8	362 ± 19	144	331

Table 4 (contd.)

Grain spot	Type[a]	f[b] %	Ratios corrected for common Pb:		Apparent ages (Ma):		Th (ppm)	U (ppm)
			$\frac{^{206}Pb^{c}}{^{238}U}$	$\frac{^{207}Pb^{d}}{^{235}U}$	$\frac{^{206}Pb^{c}}{^{238}U}$	$\frac{^{207}Pb^{d}}{^{235}U}$		
ISO4-105.1	Mag	0.4	0.04239 ± 0.00059	0.2871 ± 0.0115	268 ± 4	256 ± 9	255	924
ISO4-105.2	Mag	1.1	0.04335 ± 0.00069	0.2787 ± 0.0120	274 ± 4	250 ± 10	55	604
ISO4-109.1	Mag	0.0	0.04623 ± 0.00056	0.3006 ± 0.0090	291 ± 3	267 ± 7	182	1027
ISO4-109.2	Mag	0.5	0.04860 ± 0.00095	0.3039 ± 0.0237	306 ± 6	269 ± 18	218	374

[a] *Prism* prismatic overgrowth, *stub* stubby overgrowth, *isom* isometric overgrowth, *leuc* leucosome growth, *ZCA* zoning-controlled alteration, *SCA* surface-controlled alteration, *core br* inherited core with strong cathodoluminescence

[b] Percent of total ^{206}Pb which is non-radiogenic
[c] Common Pb correction based on ^{207}Pb
[d] Common Pb correction based on ^{208}Pb

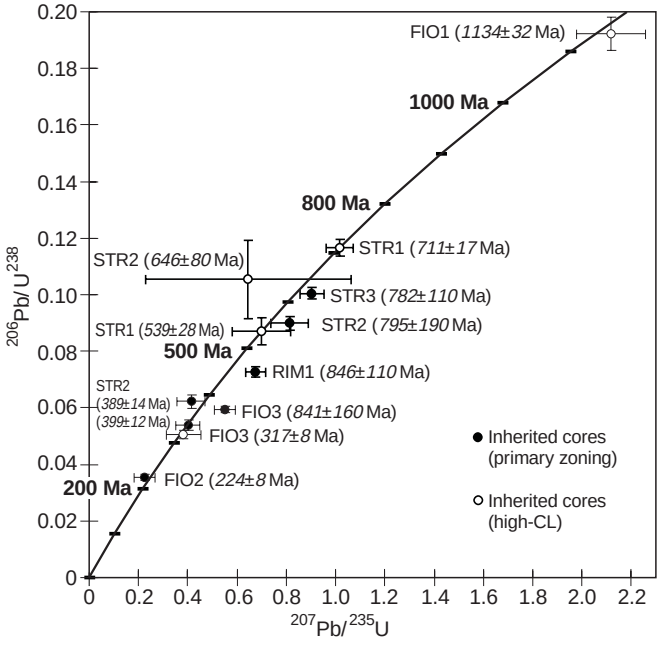

Fig. 4 Concordia plot of $^{206}Pb/^{238}U$ data and $^{207}Pb/^{235}U$ data from inherited zircon cores in metasedimentary and meta-igneous samples. *Values in parentheses* are $^{206}Pb/^{238}U$ data for analytically concordant analyses and $^{207}Pb/^{206}Pb$ data for analytically discordant analyses. Errors are 2σ

Zircon genesis and significance of U-Pb ages

Growth and origin of inherited zircon cores

Inherited zircon cores occur in all metasedimentary samples and in the meta-igneous samples FIO3 and ISO4. A peculiar characteristic of many of the zircon cores, especially of those in the metasediments, is their angular shape that resulted from grain breakage (Fig. 2: 2, 7, 8, 12, 14, 19). Since typical detrital zircons from sediments are commonly thought to be rounded and pitted by abrasion, the contrary observation of grain breakage in the IZ samples requires some explanation. Small irregular zircon fragments may be a rather typical occurrence in pelitic and semipelitic rocks, because small grains are less able mechanically to interact than larger grains and so are better protected from abrasion. Most of the fractured zircon cores are very small (<50 μm). If zircons so small are present in unmetamorphosed sediments without any overgrowth, they are difficult to separate and are commonly overlooked. Small fractured grains are also produced by breakage during sample processing in the laboratory and cannot be distinguished from original detrital grai + n shapes. It is the large amount of overgrowth during high-grade metamorphism (anatexis) that helps to sample and to observe the small detrital grains and also enables identification of their broken shapes as being of detrital origin.

Although the inherited cores, with well preserved primary zoning, might be expected to have retained closed U-Pb systems representing the age of growth, the discordancy of most apparent ages (Fig. 4) indicates that the cores have been affected by one or more Pb-loss events. The age of primary growth is at least as old as the apparent $^{207}Pb/^{206}Pb$ age. Accordingly, all the discordant cores have grown in the Precambrian. Assuming that Pb-loss from the cores has occurred at the time of high-grade metamorphism (ca. 300 Ma), the upper intercepts of presumed mixing lines (discordias) indicate that at least some of the cores have grown in the Early Proterozoic or earlier, in line with conventional upper intercept ages of zircons from metasediments (Köppel 1974). Some cores with young apparent ages are analytically concordant (Fig. 4), but still may be rejuvenated by Pb-loss. The apparent U-Pb age is only a minimum age of their growth. The particular young apparent age of a zircon core in the garnetite FIO2 (Fig. 2: 18), is definitely due to Pb-loss, because some of the overgrowths in this rock, though also affected by Pb-loss, have higher apparent ages. Strongly luminescent (high-CL) cores are discussed below under the topic of alteration.

Overgrowth and new growth of zircons during high-grade metamorphism and anatexis

Zircon overgrowths of variable morphology, internal structure and Th-U chemistry are present on the detrital zircons of the restitic metasediments and, by much smaller volume, on the magmatic zircons of the meta-

igneous granulite ISO4. As an earlier zircon study (Schiotte et al. 1989) of a metamorphic sequence comprising the amphibolite–granulite facies transition has shown, zircon overgrowth in quartzo-feldspathic lithologies does not occur in most of the amphibolite facies and starts near the transition to the granulite facies. As these conditions are such as to induce anatexis in the quartzo-feldspathic lithologies of the IZ, the observed zircon growths and overgrowths, in restites, leucosomes and meta-igneous granulite, are supposed to have entirely formed in an anatectic environment.

Since the angular (detrital) shapes of the inherited cores in the metasediments were not affected by partial dissolution, the large amount of zircon constituting the overgrowth could not have been derived from dissolution of detrital zircons, at least not from partial dissolution of the crystals that have survived as inherited cores. The Zr may have been derived from the decomposition of biotite during prograde metamorphism. However, recent SIMS analyses of biotite indicate that it does not incorporate significant amounts of Zr (J. Reinhardt personal communication). An alternative and more realistic mechanism for the formation of large zircon overgrowths during anatexis in metapelites is a process that is known as Ostwald ripening. During this process, the matrix (anatectic melt) is supersaturated with respect to the larger grains, so these grow larger, and is undersaturated with respect to the smaller grains which grow smaller and may eventually disappear (Shelley 1993; p. 254). Very small dust-like grains of zircons are likely to be abundant in pelitic sediments, though this has not yet been investigated, and once they get contact with droplets of anatectic melt, they will become readily dissolved, thus supersaturating the adjacent melt where the larger detrital grains become overgrown. This will happen during the prograde path of metamorphism. The growth of zircon in a prograde environment is in fact supported by the observation that the prism-blocked and low-luminescence type of overgrowth in the upper amphibolite facies (Fig. 2: 1, 2) is present as a very small incipient stage of overgrowth on most detrital zircons at higher metamorphic grades (Fig. 2: 7, 8, 12, 13, 14, 15, 17, 18, 19, 20). The very small size (<5 μm) of this incipient stage indicates that, in the granulite facies samples, the prograde upper amphibolite facies conditions, where zircon overgrowth initiated, did not last for very long and were rapidly superseded by granulite facies conditions where stubby and isometric types of zircon overgrowths were formed.

In the variety of morphology, internal structure and Th-U chemistry of the zircon overgrowths (Figs. 2, 3), there appears to be a systematic sequence ranging from prismatic (prism-blocked) low-Th/U types (STR1r) over stubby medium-Th/U types (STR2r) to isometric high-Th/U types (STR3r, RIM1a, FIO1, FIO2, ISO4). At relatively low metamorphic grade (STR1r and STR2r), the prismatic and stubby type of overgrowth occur alone. At higher metamorphic grades (STR3r, FIO1, FIO2) the isometric type of overgrowth becomes dominant and the prismatic and stubby types are restricted to early and volumetrically minor stages of overgrowth. These observations suggest that the metamorphic grade is an important factor controlling the morphology and Th-U chemistry of the overgrowth. In addition, there exists a lithological control on the type of overgrowth, shown by the observation that in sample RIM1 overgrowth is perfectly isometric in the arenitic lithology (RIM1a), but stubby in the pelitic lithology (RIM1p).

Any explanation of the morphological variability of overgrowths, in terms of environmental factors, must consider that the morphology is the expression of the stability and the relative growth rates of crystal faces. The observed range of crystal habits (prismatic, stubby, isometric) corresponds to a decreasing stability of planar crystal faces. Where planar crystal faces are stable throughout, the resulting habit is prismatic (Fig. 2: 1, 2, 7, 8, 9). Where the crystal faces become intermittantly unstable (implying intermittantly accelerated growth rates), the result is fir-tree zoning (Raven and Dickson 1989; Vavra et al. 1996) and a stubby habit (Fig. 2: 3, 4, 5, 6, 10, 11, 16). Where planar crystal faces become unstable altogether, the growth morphology becomes isometric and roundish (Fig. 2: 12, 13, 14, 16, 19, 31). According to crystal growth theory, the transition from stability to instability of planar crystal faces results from a switch in the growth mechanism from layer growth to continuous (adhesive) growth (Dowty 1980), also known as kinetic roughening (Sunagawa 1987). The theory of a switching growth mechanism provides explanations for unsteady growth rates in the fir-tree zoning and for the abrupt transition from prismatic to isometric habits observed in some crystals (Fig. 2: 7, 8, 16, 17, 20). It may also provide a plausible explanation for the large (one order of magnitude) gap of Th/U ratios between the prismatic or stubby overgrowths, on the one hand, and the isometric overgrowths, on the other hand (Fig. 3). It is possible that the low Th/U ratios (<0.1) in the prismatic and stubby zircons correspond more closely to the equilibrium distribution coefficients (Th being more incompatible in zircon than U; Speer 1982) than the much higher Th/U ratios (near 1) in the isometric overgrowths. The latter may be the result of the kinetically fast and chemically less selective continuous growth mechanism, making the Th/U ratio in the crystal more similar to that of the environment where it is commonly larger than 1 (Faure 1986). The environmental factors causing zircon crystal faces to be more or less stable remain hypothetic. A dependence on temperature may explain the rough correlation of morphology with the metamorphic grade. But the observed control by lithology (RIM1p and RIM1a) requires an alternative factor and this is, probably, the activity of H_2O in the anatectic melt. Theoretical considerations of the surface energies of the crystal faces of zircon (Woensdregt 1992) predict that the {110}-prism faces are stabilized and reduced in growth rate by adsorbing H_2O. This is compatible with the high stability and very low growth rates of the {110}-prism faces in the amphibolite facies anatectic melt

(Fig. 2: 1, 2) which is probably H_2O-saturated. At the extreme opposite, the anatectic melt in the dry lithologies of the granulite facies (meta-arenite RIM1a and meta-igneous granulite ISO4) is supposed to be the most H_2O-undersaturated. In these lithologies the zircon overgrowth is isometric (Fig. 2: 12–14, 29–31).

In addition to H_2O-activity, supersaturation of the anatectic melt is also expected to influence the growth morphology (Sunagawa 1987) and this factor may have to be invoked to explain the generally greater stability of crystal faces in the leucosome zircons (Fig. 2: 6, 9) as compared to the restite zircons (Fig. 2: 3, 4, 8). No matter what the real environmental parameters causing the large morphological and chemical diversity are, the point that is most important for the interpretation of radiometric data is the different resistance of the distinguished overgrowth types to alteration processes and Pb-loss, a point to be discussed in the next section.

In order to date the primary crystallization age of the anatectic zircon overgrowths and growths in restites and leucosomes, only crystal domains that are free of visible alterations (ZCA and SCA) are considered (filled square and diamond symbols in Figs. 3 and 5). The distribution of apparent ages in Fig. 5 shows that even the restriction to visibly unaltered domains does not isolate undisturbed U-Pb systems. There is a significant excess scatter of apparent ages, spanning tens of million

Fig. 5 Apparent $^{206}Pb/^{238}U$ ages and U concentrations of metamorphic (anatectic) and magmatic zircons. Errors are 2σ. (*ZCA* zoning-controlled alteration, *SCA* surface-controlled alteration). For explanation of symbols see legend in Fig. 3

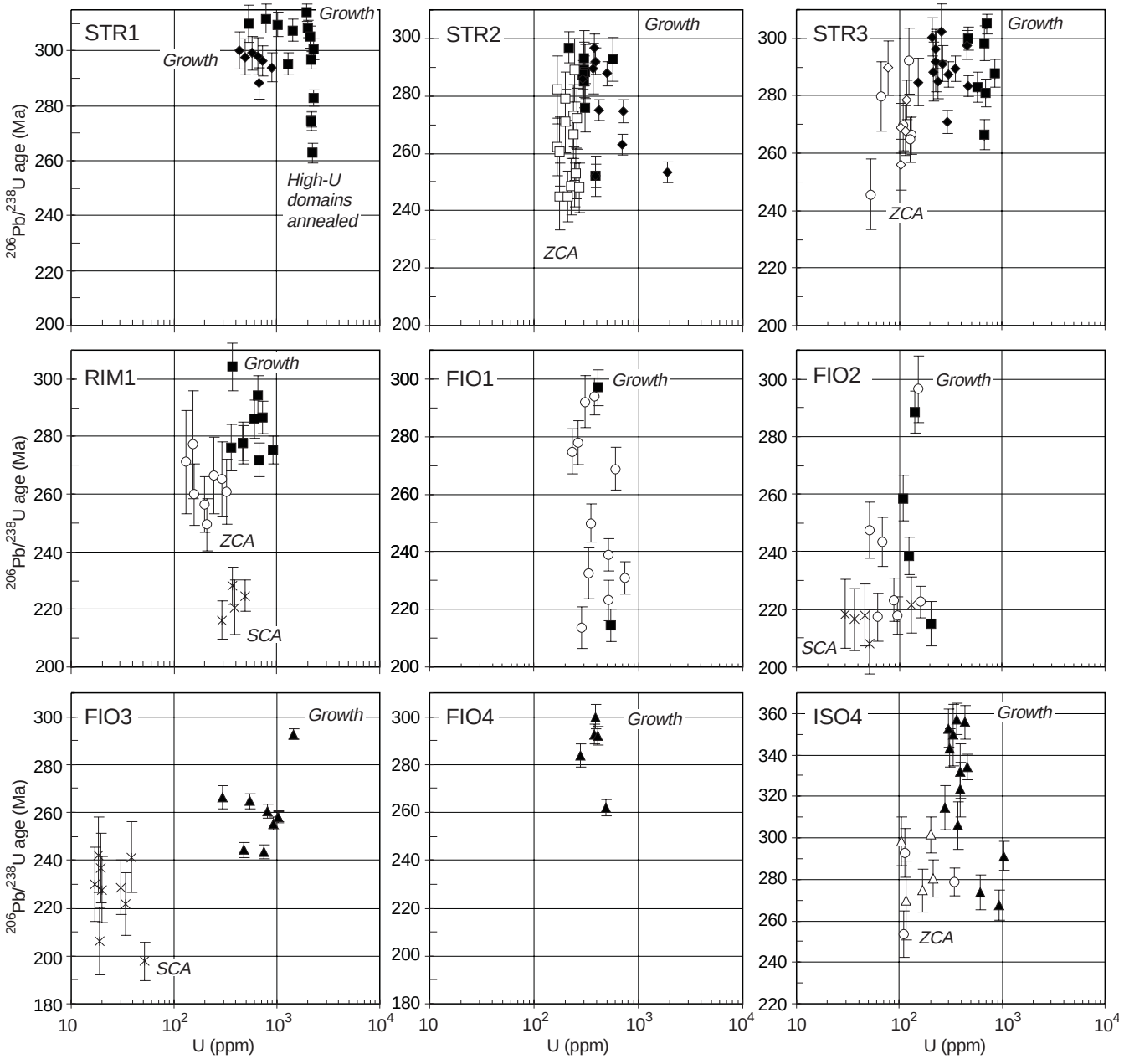

years, even within single growth generations within single samples. The possible explanation that the overgrowth has formed in successive steps during an interval of time spanning several tens of million years is invalidated by the observation that, in many overgrowths, inner zones are apparently younger than outer zones (Fig. 2: 16). Therefore, the range of apparent ages results from one or several events of Pb-loss and the highest apparent ages from several samples provide a minimum age for the primary crystallization. It is remarkable that the highest apparent ages of overgrowth and growth domains obtained from every restite and leucosome sample, with the only exception of STR1r, are identical (Fig. 5; Table 5). Considering this coincidence of the highest apparent ages from 9 samples, the weighted mean of 299 ± 5 Ma (95% confidence limit) is interpreted as the real age of zircon growth and overgrowth in restites and leucosomes. This is supported by the fact that, in samples STR2 and STR3, most of the apparent ages cluster at or just below 299 Ma. In sample STR1r, the group of the highest apparent ages yields a mean age of 310 ± 6 Ma (95% c. l.) suggesting that the anatectic overgrowth in this metasedimentary restite started earlier than anatectic growth and overgrowth in all the other restite and leucosome samples (299 ± 5 Ma). The difference of age between sample STR1r and the other samples is, however, on the edge of significance and must be verified by further investigations.

Magmatic crystallization of zircons in the meta-igneous rocks

The metagabbro (FIO3) and the metaperidotite (FIO4), both part of the Mafic Formation, contain zircons with shapes, internal structures and Th/U ratios (ca. 0.3) typical of magmatic crystallization. The zircons of the metagabbro are relatively rich in U, compatible with the crystallization of a gabbroic cumulate where zircon crystallization is deferred until the residual liquid becomes enriched in U. The very simple magmatic shapes of the zircons in the metaperidotite, D-type according to Pupin (1980), suggest that it also originated as a cumulate rock. Metagabbro and metaperidotite may be cogenetic. Considering that the spread of apparent ages from magmatic zircon domains (Fig. 5: FIO3, FIO4; triangles) exceeds the analytical uncertainty, most if not all analyses represent mixtures of ages comprising growth and one or more Pb-loss events. In both samples, the age of magmatic growth is at least as old as the oldest apparent age, i.e. 293 ± 6 Ma (2σ) in the metagabbro and 300 ± 6 Ma (2σ) in the metaperidotite. Since these apparent ages coincide with the age of 299 ± 5 Ma that was derived for the anatectic overgrowth and growth of zircons in the restitic metasediments and leucosomes (Table 5), they support the assumption of a genetic context between mafic/ultramafic underplating and anatexis in the IZ.

The main zircon population in the meta-igneous granulite (ISO4) also shows typical magmatic characteristics with respect to Th/U ratio (ca. 0.3) and euhedral prismatic zoning. Prominent development of the steep pyramidal faces {121} (Fig. 2: 29, 30), the ubiquitous presence of small inherited cores (Fig. 2: 30, 31), the enrichment of U towards outer growth zones (low-luminescence zones in Fig. 2: 29, 30), and the presence of internal rounded resorption stages (Fig. 2: 31) are indicative of a calcalkaline affinity of the magma (Vavra 1994), which is in accordance with the bulk rock chemistry of the parent rock (Vavra et al. 1996). The apparent ages from magmatic zircon domains again show a large scatter due to one or more episodes of Pb-loss (Fig. 5: ISO4; filled triangles). The minimum age of crystallization is therefore represented by the group of highest apparent ages (355 ± 6 Ma; 95% c. l.). It predates the Late Carboniferous magmato-metamorphic event in the IZ. If the protolith of the meta-igneous granulite was deposited in a volcano-sedimentary environment, as suggested by the admixture of a minor subpopulation of metasedimentary zircons (Fig. 2: 16 in Vavra et al. 1996), the age of 355 ± 6 Ma is a maximum age of deposition.

Zircon alterations and mechanisms of Pb-loss

The large dispersion of apparent U-Pb ages (Fig. 5) shows that the majority of zircon domains, from magmatic as well as from anatectic growth generations, were affected by Pb-loss causing differential rejuvenation. The recognition and age discrimination of Pb-loss events pose two fundamental problems in addition to those already involved in the dating of primary growth. Whereas any growth or overgrowth of zircon is entirely controlled by the environment (magmatism or anatexis), Pb-loss is controlled by both environmental ingredients and susceptibility of the crystals. The geological significance of any Pb-loss event depends on the relative weights of these parameters. The second problem resides in the discrimination between distinct Pb-loss events within a range of apparently concordant data. Whereas the growth of any crystal domain is a single event, with a minimum age constrained by the highest apparent age, Pb-loss may be multi-episodic and the only mathematical constraint of its age is that the latest Pb-loss is as young or younger than the lowest apparent age. Since discordancy cannot be discerned, any apparent age in the range may represent either a real age of Pb-loss or a mixture of ages involving growth and one or several Pb-loss events.

Pb-loss due to radiation damage of high-U domains

The commonly applied conception that radiation dosage (metamictization), due to high-U content and exposure time, is the major agent of Pb-loss from zircon (see re-

view by Mezger and Krogstad 1997), is not supported by most of the present patterns of rejuvenated U-Pb ages. The zircons were relatively young at the time of Pb-loss and most of the analyzed domains have fairly low U concentrations of less than 700 ppm, and still they became heavily affected by Pb-loss. A negative correlation between apparent ages and U concentration, indicating Pb-loss controlled by radiation damage (Silver and Deutsch 1963), can only be recognized in the U-rich zircon overgrowths of the amphibolite facies metapelite STR1r (Fig. 5). In this sample, significant Pb-loss is restricted to U concentrations of 2000 ppm and above. The existence of a threshold value of U content, above which Pb-loss becomes important, has been reported by Williams (1992) and may be a characteristic of Pb-loss induced by radiation damage. The threshold content reported by Williams is only about 700 ppm U. There is, however, no reason to assume that it has to be the same for every sample. Low-Th/U zircons, as they occur in sample STR1, have been repeatedly reported as being especially resistant against Pb-loss, even at high-U concentrations (Schiotte et al. 1989; Williams 1992; Williams et al. 1996).

In the granulite facies samples, the expected correlation between U concentration and Pb-loss is not obvious. There is at most a tendency for U-rich domains of 1000 ppm U and above to be rejuvenated, yielding similar apparent ages around 260 Ma (Fig. 5: STR2, FIO3, ISO4; Table 5) comparable to the youngest apparent age of the U-rich zircon overgrowth in the amphibolite facies sample STR1.

Since Pb-loss from high-U zircon domains is dominantly controlled by the susceptibility of the crystal lattice, the rejuvenated ages do not necessarily correspond to a geologically important event. However, the near coincidence of several young apparent ages from U-rich domains (Table 5) may result from near-complete resetting during an episode of annealing. Annealing of radiation damage in high-U domains is also indicated by the clearness and transparency of the investigated crystals, not showing any evidence of metamictization. Annealing is associated with episodic Pb-loss (e.g. Pidgeon et al. 1973; Gebauer and Grünenfelder 1976) and can be induced already at relatively low temperatures (ca. 300–500 °C).

Although Pb-loss due to annealing of a radiation-damaged lattice may have been significant for some U-rich zircon domains, it has not caused any noticeable effect neither in the CL patterns (dark domains in Fig. 2: 1, 2, 29, 30), nor in the Th-U chemistry (Fig. 3: STR1, FIO3, ISO4). In the following, two alternative and volumetrically more important mechanisms of Pb-loss are discussed. These have caused strong changes in luminescence and Th-U chemistry.

Pb-loss due to zoning-controlled alteration (ZCA)

Where ZCA domains can be distinguished from adjacent unaltered domains, as in the stubby overgrowth of STR2r (Fig. 2: 3–5; Fig. 5: filled and open squares), in the leucosome growth of STR3l (Fig. 5: filled and open diamonds) and in the magmatic growth of ISO4 (Fig. 2: 29–31; Fig. 5: filled and open triangles), the ZCA domains are more strongly affected by Pb-loss and rejuvenation than the unaltered domains. Since ZCA is also characterized by U-loss (Fig. 3: STR2, STR3, ISO4), there exists a positive correlation between U concentration and apparent U-Pb age (Fig. 5: STR2, STR3, ISO4) which is reverse to the negative correlation that characterizes Pb-loss induced by radiation damage and annealing (Fig. 5: STR1).

In most cases of isometric overgrowth (Fig. 2: 7, 8, 12, 15–17, 19, 20, 29, 30), ZCA domains cannot be discerned from unaltered domains, because most of this overgrowth type is highly luminescent and, if luminescence contrasts occur, like in Fig. 2: 13, 14 and 31, they do not correlate with apparent ages and loss of Th and U. It is however observed that the isometric overgrowths as a group are more rejuvenated than the unaltered stubby and prismatic domains within the same sample (Fig. 5: STR3 and RIM1; circles). This suggests that the ZCA-related Pb-loss affected almost all of the isometric overgrowth, whereas it affected only part of the stubby overgrowth in STR2r, the leucosome growth in STR3l, and the magmatic growth in ISO4.

Patchy domains of alteration within zircon crystals, with morphological and chemical characteristics similar to the described ZCA domains, have been reported in a number of earlier microanalytical investigations of granulite zircons (e.g. Black et al. 1986; Schiotte et al. 1989; Williams 1992; Pidgeon 1992). These authors have referred to these domains as recrystallized, using this term in a purely descriptive way. In every case, the origin of this type of alteration was ascribed to high-grade thermal events. For example, Schiotte et al. (1989) and Williams (1992) noted that recrystallization is present in granulite facies zircons, but is absent in the amphibolite facies ones. Since in the IZ the zircons grown during the granulite facies are themselves affected by ZCA (recrystallization), it is implied that high-grade metamorphic conditions recurred tens of million years after the Upper Carboniferous (299 ± 5 Ma) first high-temperature event and anatexis. However, the susceptibility of the crystal lattice must be considered as an alternative factor causing ZCA. One might suspect that high U concentrations causing metamictization, followed by annealing and Pb-loss, have also promoted ZCA. This is not supported by observation, because the U-richest domains, including upper amphibolite facies zircon overgrowth in sample STR1 (Fig. 2: 1, 2), the magmatic zircons of the metagabbro FIO3 (Fig. 2: 23–25), and the late growth stages of the magmatic zircons in the metaigneous granulite ISO4 (Fig. 2: 29, 30) are not affected by ZCA. Nevertheless, ZCA is strongly controlled by some structural or chemical attribute of the crystal lattice, because the distinguished morphological types of zircon overgrowth show greatly different susceptibilities to ZCA. The prism-blocked low-Th/U overgrowths are

the most resistant (Fig. 2: 1, 2). The stubby medium-Th/U overgrowths are partly and very selectively altered, mostly near sector boundaries and inclusions (Fig. 2: 3–6). The isometric high-Th/U overgrowths appear to be the most altered with only faint relics of primary structures (Fig. 2: 7, 8, 12, 13, 14, 16, 17, 20, 31) being left.

The different susceptibility of the distinguished overgrowth types is observed in single samples and even in single grains (Fig. 2: 7, 8, 17, 20). What exactly causes the isometric overgrowth especially to be prone to ZCA remains speculative. As already remarked, the switch of growth mechanism from layer growth to continuous growth can explain the transition from prismatic to isometric habit and concomitant increase in the Th/U ratio. It is tempting to speculate that the continuous growth mechanism also causes imperfections in the crystal lattice that later becomes prone to ZCA.

Considering that the susceptibility of the crystal lattice is an important factor causing ZCA, at least in the case of the isometric overgrowth, the interpretation of ZCA in terms of significant geological events becomes doubtful. However, earlier investigations that relate zircon recrystallization (ZCA) to high-temperature events (Black et al. 1986; Schiotte et al. 1989) have not referred to isometric zircon overgrowths, but to prismatic magmatic zircons in meta-igneous rocks, comparable to those in the meta-igneous granulite ISO4 (Fig. 2: 29–31). The magmatic zircons of this sample grew before 355 Ma (Fig. 5) and, in any case, before the major granulite facies thermal event at 299 ± 5 Ma. The influence of temperature as an agent of ZCA is supported by two apparent ages (298 ± 12 Ma and 302 ± 8 Ma; 2σ), from ZCA domains, that are compatible with the 299 Ma age of granulite facies metamorphism (Fig. 5: ISO4; unfilled triangles with highest apparent ages). Assuming that the susceptibility of the crystal lattice was the dominant factor causing ZCA, we should expect that all susceptible crystal domains had been affected already during the granulite facies metamorphism at 299 Ma. No apparent age should be younger, because crystal domains, once they are recrystallized, become extremely resistant against further Pb-loss during later high-temperature events (Schiotte et al. 1989; Pidgeon 1992). However, three apparent ages (270 ± 20 Ma, 275 ± 10 Ma and 281 ± 8 Ma; 2σ) from ZCA domains within magmatic growth are significantly younger than 299 ± 5 Ma (Fig. 5: ISO4) and indicate the presence of at least one further event after the Upper Carboniferous granulite facies metamorphism, causing additional ZCA of not yet altered domains. This also supports that the ZCA found in the granulite facies zircon overgrowths has been induced by geological events and is not merely due to strong susceptibility of the crystal lattice. It must be remarked that, although recrystallization of zircon (called ZCA in this investigation) has previously been ascribed to high temperatures (Schiotte et al. 1989; Williams 1992; Pidgeon 1992), its origin by other geological events, e.g. decompression, has not been investigated and, therefore, must also be considered.

The interpretation of the large dispersion of apparent ages from ZCA domains (open symbols in Fig. 5) is ambiguous. The dispersion is due either to multiple events or to differential Pb-loss during only one single event. In any case, the youngest event causing ZCA is as young or younger than the lowest apparent age. Aside from the samples of Val Fiorina (FIO1, FIO2 and FIO3), where zircons were strongly overprinted by a much later fluid infiltration to be discussed below, one notes that the youngest apparent ages from ZCA domains of the remaining samples (Fig. 5: STR2r, STR3r, STR3l, RIM1a and ISO4; unfilled symbols) coincide and yield a mean age of 249 ± 7 Ma (Table 5). This coincidence of the youngest apparent ages from ZCA domains of several samples and the fact that they are younger than the youngest apparent ages from high-U domains (Table 5) can hardly be fortuitous. The probable interpretation is that a major episode of ZCA occurred at a strong thermal and/or decompression event at 249 ± 7 Ma. The less effective rejuvenation of U-rich domains may result either from annealing having occurred earlier at a lower temperature than ZCA or from Pb-loss by annealing being generally less effective (incomplete) than Pb-loss by ZCA.

The inherited zircon cores that are strongly luminescent (Fig. 2: 1, 2, 10, 12, 15, 19, 24, 25) have probably been affected by the same alteration mechanism (ZCA). Whereas most cores with unaltered primary zoning are discordant (Fig. 4), indicating that Pb-loss was only partial, all the high-CL cores are concordant, probably due to nearly complete Pb-loss and extinction of earlier age components during ZCA. The alteration of three inherited cores with apparent ages of 539 ± 28 Ma, 711 ± 17 Ma and 1134 ± 32 Ma (2σ) occurred much earlier than the granulite facies metamorphism in the IZ. It must have been produced under high-grade metamorphic conditions in the source area of the detrital zircons, and not after their deposition in the IZ. If they were already deposited in the pelitic rocks of the IZ, the early high-grade events causing ZCA of detrital zircons would also have induced anatexis of the pelites, which, in turn, would have given rise to voluminous zircon overgrowth. However, zircon overgrowths significantly older than 299 ± 5 Ma (310 ± 6 Ma only in STR1r) have so far not been detected in the IZ.

Pb-loss due to surface-controlled alteration (SCA)

Since this second type of zircon alteration with bright crystal rims (Fig. 2: 11, 21, 22, 26, 27) starts at corroded crystal surfaces and is unselective with respect to primary structures and morphologies, ingression of and leaching by fluids rather than temperature and susceptibility of the crystal lattice must be considered as the major agents. The preponderence of fluid over thermal action is supported by the localized occurrence of this type of

alteration. It is strongest in the samples FIO1, FIO2 and FIO3 from the 10 m wide profile at the Fiorina river and, even here, varies at the scale of a few meters, being stronger in sample FIO2 (garnetite) and FIO3 (metagabbro) than in sample FIO1 (metapelite). In sample FIO1 CL-bright crystal rims are not observed and the evidence of alteration is limited to the very faintness of internal growth structures. Within the samples FIO2 and FIO3, the individual zircon crystals are affected by SCA to very variable extents (Fig. 2: 18–27).

According to hydrothermal experiments (Pidgeon et al. 1966), and empirical evidence (Friend and Nutman 1992), H_2O and CO_2 of metamorphic fluids are not expected to cause any significant alteration and Pb-loss in zircons. However, fluids containing sufficient amounts of certain ingredients, like F, Cl, Na, Ca, can be very aggressive causing severe alteration and Pb-loss even from unmetamict zircons at low temperatures within a few hours (e.g. Hansen and Friderichsen 1989; Sinha et al. 1992). The experiments of Sinha et al. (1992) have demonstrated that leaching of Pb by aggressive fluids from unmetamict zircons is episodic rather than continuous, because the rate of leaching decreases rapidly after a few hours of hydrothermal treatment.

Considering that the granulite zircons of the IZ were already rejuvenated by one or several episodes of ZCA related to thermal pulses and/or decompression, one may doubt whether it is possible to isolate fluid-induced SCA as a separate age. Fortunately, SCA was a local process, and only samples that were affected (RIM1p, FIO1, FIO2, FIO3) yield apparent ages significantly younger than the 249 ± 7 Ma age of ZCA (Fig. 5). Consequently one or possibly several SCA events postdated ZCA. The last SCA event was as young or younger than the lowest apparent ages. Since the youngest apparent ages from SCA domains of four samples (RIM1p, FIO1, FIO2, FIO3) coincide and the youngest apparent ages in the garnetite sample (FIO2) form a distinct cluster (Fig. 5), the mean of the youngest apparent ages taken from each sample (210 ± 12 Ma; Table 5) is considered as the best estimate of the real age of SCA.

The distribution of the apparent ages from the Val Fiorina samples (FIO1, FIO2, FIO3) shows that strong rejuvenation due to fluid action is not restricted to the corroded and CL-bright crystal rims (Fig. 2: 21, 22, 26, 27; Fig. 5: crosses), but is also present in domains where the growth zoning is faint but still preserved (Fig. 2: 15, 16, 18, 19; Fig. 5: FIO1, FIO2, filled squares). Also, the isometric overgrowths in samples FIO1 and FIO2, that may have already recrystallized at 249 ± 7 Ma (Fig. 2: 15–17, 19, 20), became partially rejuvenated by later fluid action at 210 ± 12 Ma (Fig. 5: FIO1, FIO2, circles).

Implications for protolith genesis and tectono-metamorphic evolution of the Ivrea Zone

Metamorphic and magmatic climax

The microanalytical U/Pb ages of newly grown zircon in restitic metasediments and associated leucosomes, and of magmatic zircons in mafic and ultramafic intrusions (Table 5) support the hypothesis first proposed by Schmid (1967) that the amphibolite to granulite facies metamorphism in the IZ accompanied by anatexis was induced by magmatic underplating. It confirms the general assumption (since Pin 1986) that all of this happened in the Late Carboniferous. The age of 299 ± 5 Ma, derived from the highest (least rejuvenated) apparent ages, is strictly speaking a minimum age for the beginning of magmatism and high-grade metamorphism in the IZ and probably represents a short lived event of large regional extent. The latter interpretation is supported by the fact that the age of 299 ± 5 Ma from

Table 5 Summary of U-Pb zircon ages (Ma). Errors of single analyses: 2σ; errors of means of analyses: 95% confidence level; errors comprise counting errors and calibration uncertainty

Sample	Anatectic growth	Magmatic growth	High-U domains	Zoning-controlled alteration	Surface-controlled alteration
STR1r	310 ± 6 (n = 6)	–	263 ± 4	–	–
STR1l	297 ± 5 (n = 4)	–	–	–	–
STR2r	297 ± 6	–	–	248 ± 5 (n = 6)	–
STR2l	297 ± 6	–	253 ± 4	–	–
STR3r	305 ± 6	–	–	246 ± 12	–
STR3l	302 ± 10	–	–	256 ± 9	–
RIM1p	304 ± 8	–	–	–	216 ± 7
RIM1a	–	–	–	249 ± 9	–
FIO1	297 ± 6	–	–	–	214 ± 7
FIO2	296 ± 11	–	–	–	208 ± 11
FIO3	–	293 ± 6	258 ± 4 (n = 4)	–	199 ± 11
FIO4	–	300 ± 6	262 ± 4	–	–
ISO4	293 ± 12	355 ± 6 (n = 4)	266 ± 7	254 ± 11	–
Mean	299 ± 5[a]				
	300 ± 5[b]	–	–	249 ± 7	210 ± 12

[a] STR1r excluded from calculation of the mean
[b] STR1r included in calculation of the mean

the least rejuvenated crystal domains of newly grown zircon is the same in restites and leucosomes and in all samples extending across a considerable part of the IZ, comprising deeper and more shallow crustal levels. The evidence of a strong, short lived and regionally extended magmatism and anatexis at 299 ± 5 Ma points to an important geotectonic event, for example the delamination of the lithospheric mantle as proposed by Pin (1990).

Pre-climax history

The zircons that are now present as detrital zircon cores in the metasediments grew in the Proterozoic and became partially recrystallized during Late Proterozoic and Early Paleozoic high-grade metamorphic events in their source rocks (Fig. 4). Since these high-grade metamorphic events have occurred in the source rocks rather than in the IZ, the youngest age of recrystallization obtained from a zircon core (Fig. 4: 539 ± 28 Ma) in a metasediment has to be considered as a maximum age for both erosion of the source rock and deposition in the IZ sediments. Apparent ages obtained from a young and unrecrystallized zircon core (389 ± 14 Ma) in a metapelite (Fig. 4: STR2) and from magmatic zircons (355 ± 5 Ma) in a meta-igneous granulite (Fig. 5: ISO4) of possibly volcano-detrital origin suggest that parts of the IZ may have been deposited as late as the Devonian or Early Carboniferous. The age of 355 ± 5 Ma from the meta-igneous granulite is as yet the highest reliable age for the formation of a rock in the IZ. It remains the subject of further radiometric investigation to check whether the accretion of the continental crust represented by the IZ started earlier than 355 ± 5 Ma.

Further evidence of a young magmato-metamorphic evolution of the IZ relative to the SCZ comes from the observation that none of the overgrowths on detrital zircons in the metasediments, none of the zircons in the leucosomes, and none of the zircons in the mafic and ultramafic intrusions are, as far as is shown by the available samples, significantly older than the age of 299 ± 5 Ma (310 ± 6 Ma only in STR1r). Especially, the voluminous overgrowth of detrital zircons in the metasediments is regarded as a sensitive tracer of the very first attainment of the solidus temperature during high-grade metamorphism, and this has not occurred earlier than 299 ± 5 Ma in the investigated parts of the IZ. This has some important bearings on the tectonic relationship between the IZ and SCZ in Variscan and pre-Variscan times. If the SCZ were affected by high-grade metamorphism and anatexis in the Ordovician, as suggested by Köppel and Grünenfelder (1971) and by Romer and Franz (1998), the IZ was not its lower crustal continuation, but either had not yet accreted or occupied a laterally different position where the metamorphic grade was below anatexis. Even if the SCZ were not affected by Early Paleozoic high-grade metamorphism, as suggested by Boriani and Villa (1997), it doubtless has been intruded by a large volume of Ordovician granitoids which would have heated up underlying crustal parts. But no evidence of Ordovician magmatism and metamorphism of sediments has yet been found in the IZ apart from Rb-Sr and Sm-Nd whole rock data that cannot be interpreted reliably.

The problem of the situation of the IZ relative to the SCZ during the Variscan orogeny is challenging. The SCZ was affected by middle amphibolite facies metamorphism (ca. 550 °C) at 341 ± 6 Ma (Boriani and Villa 1997), and if the geothermal gradient was between 15 and 30 °C/km, a very likely situation for a Barrovian type of metamorphism, the solidus of pelitic and semipelitic lithologies (ca. 700 °C) would have been reached between 5 to 10 km below the SCZ. Since evidence of zircon overgrowth much older than 299 ± 5 Ma is absent in our investigated metasediments, the IZ with its presently observed thickness of about 10 km did not represent the lower crustal continuation of the SCZ, when the latter experienced its Variscan metamorphic climax at 341 ± 6 Ma. Amalgamation of the IZ and SCZ occurred later, and may be dated by the intrusion age of around 285 Ma (Boriani et al. 1992, and references cited therein) of the numerous igneous dykes and bodies on both sides of the CMB line (Zurbriggen 1996).

We also conclude that the stages of deformation in the IZ that pre-date the metamorphic climax (299 ± 5 Ma) were not associated with anatexis. On the other hand, amphibolite facies and lower grades of metamorphism, as long as they were not favorable for anatectic melting, may have occurred at any time without being detected in the zircon record.

Post-climax history

The U-Pb system of zircons in the IZ became disturbed by several events in the Permian, Triassic and possibly early Jurassic, causing annealing of high-U domains, temperature- or decompression-induced ZCA and fluid-induced SCA. Although similar mechanisms of alteration have not yet been investigated and therefore also not found in other minerals, the present results from zircons make it questionable that any of the radiometric data from U-Pb in monazite, Sm-Nd in garnet, and K-Ar in hornblende (Table 1) represent true cooling ages of the IZ. The complex pattern of post-climax zircon rejuvenation cannot completely be resolved, but it is possible to distinguish between two fundamentally different processes, (1) ZCA of interior crystal parts due to high-grade thermal and/or decompression pulses; (2) SCA of crystal rims due to the infiltration of aggressive fluids.

From the present data, it appears that the first process is confined to the Permian and was terminated by or consisted of a single major event at 249 ± 7 Ma. Apparent ages younger than this have not been found in any of the ZCA zircon domains of the investigated

samples, unless they were clearly affected by later fluid infiltrations. This does not exclude that later thermal pulses may have occurred, associated with sporadic Triassic and Jurassic igneous intrusions (see zircon formation ages in Table 1), but at the regional scale their thermal input was probably insignificant. Other mineral ages in the IZ that are identical to the age of ZCA (249 ± 7 Ma) and may result from the same regional events comprise a Sm-Nd internal isochron (248 ± 8) from a metabasite of Val Sesia (Voshage et al. 1987), two Ar-Ar hornblende ages (243 ± 1 Ma) from Val Strona and one Ar-Ar hornblende age (ca. 243 Ma) from the metadiorite of Val Mastallone (Boriani and Villa 1997). Reliable evidence of magmatic activity near the Permian/Triassic boundary is rare, comprising for example an albite granite with a crystallization age of magmatic zircon of 251 ± 2 Ma (Table 1; Wright and Shervais 1980). The albite granite crystallized at the border of the Balmuccia ultramafic complex in Val Sesia.

The second major mechanism of zircon rejuvenation, SCA at 210 ± 12 Ma, appears to be mirrored by a large number of other radiometric data in the IZ, from Sm-Nd internal isochrons, Ar-Ar in hornblende and Re-Os in ore minerals (Table 1). Recently, a monazite age of 210 ± 14 Ma has been obtained from sample FIO1 (Vavra and Schaltegger in this volume), coinciding with rejuvenated zircon ages in the same sample. The coincidence of ages from several isotopic systems with different closing temperatures and the absence of a clear correlation between age and metamorphic gradient in the field argues against their interpretation as cooling ages and in favor of fluid-induced resetting. In the case of hornblende, the role of local fluid-assisted recrystallization in the Upper Triassic (217 ± 1) and Lower Jurassic (183 ± 2) has been demonstrated by Boriani and Villa (1997). Aside from the regional resetting of radiometric ages, the Upper Triassic/Lower Jurassic fluids have caused metasomatism in some parts of the IZ, for example in the phlogopite peridotite of the Finero mafic/ultramafic complex (in the NE continuation of the IZ not shown in Fig. 1). The age of zircon growth (207 ± 5 Ma; von Quadt et al. 1993) within a chromitite layer of the phlogopite peridotite may directly date this metasomatism. Further evidence of Upper Triassic/Lower Jurassic fluid action in the IZ may have been largely overlooked. The pegmatitic oligoclasite dykes in mafic and ultramafic granulite facies rocks of the IZ, formerly thought to represent true magmatic rocks (Stähle et al. 1990), may have in fact crystallized from alkaline fluids rather than from melts. Crystallization ages of zircon within the oligoclasites of the Finero mafic/ultramafic complex are 225 ± 13 Ma (Stähle et al. 1990), 212.5 ± 0.5 Ma (Oppizi and Schaltegger personal communication), 201.5 Ma and 198 ± 2 Ma (Avon Quadt personal communiction). Since these ages do not coincide, several episodes of fluid circulation in the Upper Triassic/Lower Jurassic are indicated.

It seems that the two major mechanisms and episodes of zircon rejuvenation, ZCA induced by thermal and/or decompression pulses in the Permian and SCA induced by fluid ingression in the Upper Triassic/Lower Jurassic, correspond to two distinct geotectonic stages that can be discriminated in the upper crust and sedimentary cover of the Southern Alps (cf. Handy and Zingg 1991): (1) an episode of post-collisional strike-slip tectonics, basin formation and volcanism in the Permian; (2) the Upper Triassic start of continental breakup of Pangaea that was regionally associated with alkaline magmatism and hydrothermal activity not only in the Southern Alps, but also in the entire North Atlantic realm (e.g. Halliday and Mitchell 1984).

Acknowledgements We thank W. Compston and J. Foster for assisting the analytical work at the SHRIMP II at the Australian National University in Canberra, H. Hüttemann for help at the SEM in Tübingen. We also thank W. Wittwer and M. Parenti for contributions in separating the zircons at the ETH in Zürich. Rock samples FIO2 to FIO4 have been collected in a field campaign together with the Istituto di Mineralogia, Università di Modena, Italy, G. Rivalenti, M.A. Barbieri and M. Parenti. We thank our Italian colleagues for their valuable cooperation. We also thank Prof. F. Olmi (president) and G. Tallone (director) of the Parco Nazionale della Val Grande (Verbania) for the permission to collect samples and execute our field work in Val Fiorina. We very much appreciated discussions with our collegues W. Hansmann, Ch. Heinrich, V. Köppel, S.K. Matthai, U. Schaltgger, R. Stalder, A. von Quadt (all at ETH Zürich), R. Zurbriggen (Bern/Sursee), A. Ferrario (Milano) and P. Oppizzi (Lugano). We also thank I. Villa (Bern) and R.T. Pidgeon (Perth) for constructive reviews. The research work of the first author was supported by a habilitation fellowship of the German National Science Foundation. The field work and the SHRIMP analyses were financed by the Swiss National Science Foundation, projects no. 20-36049.92 (R. Schmid) and 21-31069.91 (D. Gebauer).

References

Bechstädt T, Brandner R, Mostler H, Schmidt K (1978) Aborted rifting in the Triassic of the Eastern and Southern Alps. Neues Jahrb Geol Paläontol Abh 156: 157–178

Bertotti G (1991) Early Mesozoic extension and Alpine shortening in the western Southern Alps: the geology of the area between Lugano and Menaggio (Lombardy, Northern Italy). Mem Sci Geol 43

Bertotti G, Picotti V, Bernoulli D, Castellarin A (1993) From rifting to drifting: tectonic evolution of the South-Alpine upper crust from the Triassic to the Early Cretaceous. Sediment Geol 86: 53–76

Biino GG, Meisel T (1996) Ar-Ar, Re-Os, Rb-Sr, Sm-Nd and U-Pb isotopic, trace element and petrologic study of alkaline mineralized ultramafic pipes in the Ivrea–Verbano zone (Italy). Schweiz Mineral Petrogr Mitt 76: 98–99

Black LP, Williams IS, Compston W (1986) Four zircon ages from one rock: the history of a 3930-Ma-old granulite from Mount Sones, Enderby Land, Antarctica. Contrib Mineral Petrol 94: 427–437

Boriani AC, Villa IM (1997) Geochronology of regional metamorphism in the Ivrea-Verbano Zone and Serie dei Laghi, Italian Alps. Schweiz Mineral Petrogr Mitt 77: 381–401

Boriani A, Colombo A, Macera P (1985) Radiometric geochronology of Central Alps. Rend Soc Ital Mineral Petrol 40: 139–186

Boriani A, Burlini L, Sacchi R (1990) The Cossato–Mergozzo–Brissago line and the Pogallo line (Southern Alps, N Italy) and their relationships with the late-Hercynian magmatic and metamorphic events. Tectonophysics 182: 91–102

Boriani A, Caironi V, Giobbi Origoni E, Vannucci R (1992) The Permian intrusive rocks of Serie dei Laghi (Western Southern Alps). Acta Vulcanol 2: 73–86

Brodie KH, Rutter EH (1987) Deep crustal extensional faulting in the Ivrea zone of Northern Italy. Tectonophysics 140: 193–212

Brodie KH, Rex D, Rutter EH (1989) On the age of deep crustal extensional faulting in the Ivrea Zone, Northern Italy. In: Coward MP, Dietrich D, Park RG (eds) Alpine tectonics. Geol Soc Spec Publ 45: 203–210

Bürgi A, Klötzli U (1990) New data on the evolutionary history of the Ivrea Zone (Northern Italy). Bull Swiss Assoc Pet Geol Eng 56/130: 49–70

Compston W, Williams IS, Kirschvink JL, Zichao Z, Guogan MA (1992) Zircon U-Pb ages for the Early Cambrian time-scale. J Geol Soc 149: 171–184

Dowty E (1980) Crystal growth and nucleation theory and the numerical simulation of igneous crystallization. In: Hargraves RB (ed) Physics of magmatic processes. Princeton Univ Press, Princeton, pp 419–485

Faure G (1986) Principles of isotope geology. John Wiley and Sons, New York

Ferrara G, Innocenti F (1974) Radiometric age evidences of a Triassic thermal event in the Southern Alps. Geol Rundsch 63: 572–581

Friend CRL, Nutman AP (1992) Response of zircon U-Pb isotopes and whole rock geochemistry to CO_2 fluid-induced granulite-facies metamorphism, Kabbaldurga, Karnataka, South India. Contrib Mineral Petrol 111: 299–310

Gebauer D (1993) The pre-Alpine evolution of the continental crust of the Central Alps – an overview. In: von Raumer JF, Neubauer F (eds) Pre-Mesozoic geology in the Alps. Springer, Berlin Heidelberg New York Tokyo, pp 93–117

Gebauer D, Grünenfelder M (1976) U-Pb zircon and Rb-Sr whole rock dating of low-grade metasediments – example Montagne Noire (Southern France). Contrib Mineral Petrol 59: 13–32

Gebauer D, Schmid R, von Quadt A, Ulmer P (1992) Oligocene, Permian and Panafrican zircon ages from rocks of the Balmuccia peridotite and of the Lower Layered Group in the Ivrea Zone. Schweiz Mineral Petrogr Mitt 72: 113–122

Graeser S, Hunziker JC (1968) Rb-Sr und Pb-Isotopen-Bestimmungen an Gesteinen und Mineralien der Ivrea Zone. Schweiz Mineral Petrogr Mitt 48: 189–204

Halliday AN, Mitchell JG (1984) K-Ar ages of clay-size concentrates from the mineralisation of the Pedroches Batholith, Spain, and evidence for Mesozoic hydrothermal activity associated with the breakup of Pangaea. Earth Planet Sci Lett 68: 229–239

Handy MR, Zingg A (1991) The tectonic and rheological evolution of an attenuated cross section of the continental crust – Ivrea crustal section, Southern Alps, Northwestern Italy and Southern Switzerland. Geol Soc Am Bull 103: 236–253

Hansen BT, Friderichsen JD (1989) The influence of recent Pb-loss on the interpretation of disturbed U-Pb systems in zircons from igneous rocks in East Greenland. Lithos 23: 209–223

Heaman L, Parrish R (1991) U-Pb geochronology of accessory minerals. In: Heaman L, Ludden JN (eds) Short course handbook on applications of radiogenic isotope systems to problems in geology. Mineral Assoc Can, Toronto, pp 59–102

Henk A, Franz L, Teufel S, Oncken O (1997) Magmatic underplating, extension, and crustal reequilibration: insights from a cross section through the Ivrea Zone and Strona-Ceneri Zone, Northern Italy. J Geol 105: 367–377

Hunziker JC (1974) Rb-Sr and K-Ar age determination and the alpine tectonic history of the Western Alps. Mem Ist Geol Mineral Univ Padua 31

Hunziker JC, Zingg A (1980) Lower Paleozoic amphibolite to granulite facies metamorphism in the Ivrea Zone (Southern Alps, N Italy). Schweiz Mineral Petrogr Mitt 60: 181–213

Jäger E, Niggli E, Wenk E (1967) Rb-Sr-Altersbestimmungen an Glimmern der Zentralalpen. Beitr Geol Karte Schweiz NF 134

Köppel V (1974) Isotopic U/Pb ages of monazites and zircons from the crust–mantle transition and adjacent units of the Ivrea and Ceneri zones (Southern Alps, Italy). Contrib Mineral Petrol 43: 55–70

Köppel V, Grünenfelder M (1971) A study of inherited and newly formed zircons from paragneisses and granitised sediments of the Strona–Ceneri Zone (Southern Alps). Schweiz Mineral Petrogr Mitt 51: 385–409

Köppel V, Sommerauer J (1974) Trace elements and the behavior of the U-Pb system in inherited and newly formed zircons. Contrib Mineral Petrol 43: 71–82

Lu M, Hofmann AW, Mazzucchelli M, Rivalenti G (1997) The mafic–ultramafic complex near Finero (Ivrea–Verbano Zone). II. Geochronology and isotope geochemistry. Chem Geol 140: 223–235

McDowell FW, Schmid R (1968) K-Ar ages from the Valle d'Ossola section of the Ivrea–Verbano Zone (Northern Italy). Schweiz Mineral Petrogr Mitt 48: 205–210

Mehnert KR (1975) The Ivrea zone: a model of the deep crust. Neues Jahrb Mineral Abh 125: 156–199

Mezger K, Krogstad EJ (1997) Interpretation of discordant U-Pb zircon ages – an evaluation. J Metamorphic Geol 15: 127–140

Oppizzi P, Schaltegger U (1999) Zircon-bearing plagioclasites from the Finero complex (Ivrea Zone): dating a Late Triassic mantle hic-cup? Schweiz Mineral Petrogr Mitt 79: in press

Pidgeon RT (1992) Recrystallisation of oscillatory zoned zircon – some geochronological and petrological implications. Contrib Mineral Petrol 110: 463–472

Pidgeon RT, Aftalion M (1972) The geochronological significance of discordant U-Pb ages of oval shaped zircons from a Lewisian gneiss from Harris, Outer Hebrides. Earth Planet Sci Lett 17: 269–274

Pidgeon RT, O'Neil JR, Silver LT (1966) Uranium and lead isotopic stability in a metamict zircon under experimental hydrothermal conditions. Science 154: 1538–1540

Pidgeon RT, O'Neil RJ, Silver LT (1973) Observations on the crystallinity and the U-Pb system of a metamict Ceylon zircon under experimental hydrothermal conditions. Fortschr Mineral 50: 118

Pin C (1986) Datation U-Pb sur zircons à 285 Ma du complexe gabbro–dioritique du Val Sesia–Val Mastallone et âge tardi-hercynien du métamorphisme granulitique de la zone Ivrea–Verbano (Italie). C R Acad Sci Paris Ser II 303/9: 827–830

Pin C (1990) Evolution of the lower crust in the Ivrea Zone: a model based on isotopic and geochemical data. In: Vielzeuf D, Vidal P (eds) Granulites and crustal evolution. Kluwer Academic Publishers, Netherlands, pp 87–110

Pupin JP (1980) Zircon and granite petrology. Contrib Mineral Petrol 73: 207–220

Ragettli R, Hansmann W, Köppel V (1992) U-Pb zircon and monazite ages from the Ivrea Zone and the adjoining Serie dei Laghi. U S Geol Surv Circ 1089: 15

Raven MJ, Dickson JAD (1989) Fir-tree zoning: an indicator of pulsed crystallization in calcite cement crystals. Sediment Geol 65: 249–259

Rivalenti G, Rossi A, Siena F, Sinigoi S (1984) The layered series of the Ivrea–Verbano igneous complex, Western Alps, Italy. Tschermaks Mineral Petrogr Mitt 33: 77–99

Rivalenti G, Mazzucchelli M, Barbieri MP, Schmid R, Zanetti A (1997) Garnetite-forming processes in the deep crust: the Val Fiorina case study (Ivrea–Verbano Zone, NW Alps). Eur J Mineral 9: 1053–1071

Romer RL, Franz L (1998) Ordovician Barrow-type metamorphism in the Strona–Ceneri Zone (Northern Italy) dated by U-Pb on staurolite. Schweiz Mineral Petrogr Mitt 78: 383–395

Rutter EH, Brodie KH, Evans P (1993) Structural geometry, lower crustal magmatic underplating and lithospheric stretching in the Ivrea–Verbano Zone, Northern Italy. J Struct Geol 15: 647–662

Schiotte L, Compston W, Bridgwater D (1989) Ion probe U-Th-Pb dating of polymetamorphic orthogneisses from northern Labrador, Canada. Can J Earth Sci 26: 1533–1556

Schmid R (1967) Zur Petrographie und Struktur der Zone Ivrea–Verbano zwischen Valle d'Ossola und Val Grande (Prov. Novara, Italien). Schweiz Mineral Petrogr Mitt 47: 935–1117

Schmid R (1978) Are the metapelites of the Ivrea–Verbano Zone restites? Mem Ist Geol Mineral Univ Padova 33: 67–69

Schmid R, Wood BJ (1976) Phase relationships in granulitic metapelites from the Ivrea–Verbano zone (Northern Italy). Contrib Mineral Petrol 54: 255–279

Schnetger B (1994) Partial melting during the evolution of the amphibolite-facies to granulite-facies gneisses of the Ivrea Zone, Northern Italy. Chem Geol 113: 71–101

Shelley D (1993) Igneous and metamorphic rocks under the microscope. Chapman and Hall, London

Sills JD (1984) Granulite facies metamorphism in the Ivrea Zone, N. W. Italy. Schweiz Mineral Petrogr Mitt 64: 169–191

Sills JD, Tarney J (1984) Petrogenesis and tectonic significance of amphibolites interlayered with metasedimentary gneisses in the Ivrea Zone, Southern Alps, Northwest Italy. Tectonophysics 107: 187–206

Silver LT, Deutsch S (1963) Uranium-lead isotopic variations in zircons – a case study. J Geol 71: 721–758

Sinha AK, Wayne DM, Hewitt DA (1992) The hydrothermal stability of zircon – preliminary experimental and isotopic studies. Geochim Cosmochim Acta 56: 3551–3560

Speer JA (1982) Zircon. In: Ribbe PH (ed) Orthosilicates, 2nd edn. (Reviews in mineralogy, vol 5). Mineral Soc Am Washington, DC, pp 67–112

Stähle V, Frenzel G, Kober B, Michard A, Puchelt H, Schneider W (1990) Zircon syenite pegmatites in the Finero Peridotite (Ivrea Zone) – evidence for a syenite from a mantle source. Earth Planet Sci Lett 101: 196–205

Stucki A (1998) The high grade units of the Ivrea Zone in the Ossola Valley (Province Novara, Italy). Schweiz Mineral Petrogr Mitt 78: 157–161

Sunagawa I (1987) Morphology of minerals. In: Sunagawa I (ed) Morphology of crystals. Terra Scientific, Tokyo, pp 511–587

Vavra G (1994) Systematics of internal zircon morphology in major Variscan granitoid types. Contrib Mineral Petrol 117: 331–344

Vavra G, Schaltegger U (1998) Post-granulite facies monazite growth and rejuvenation during Permian to Lower Jurassic thermal and fluid events in the Ivrea Zone (Southern Alps). Contrib Mineral Petrol (this vol)

Vavra G, Gebauer D, Schmid R, Compston W (1996) Multiple zircon growth and recrystallization during polyphase Late Carboniferous to Triassic metamorphism in granulites of the Ivrea Zone (Southern Alps): an ion microprobe (SHRIMP) study. Contrib Mineral Petrol 122: 337–358

Vogler R (1992) Die Ivreazone zwischen Val Grande und Val Pogallo (Provinz Novara, Italien). Schweiz Mineral Petrogr Mitt 72: 241–249

von Quadt A, Ferrario A, Diella V, Hansmann W, Vavra G, Köppel V (1993) U-Pb ages of zircons from chromitites of the phlogopite peridotite of Finero, Ivrea Zone, N Italy. Schweiz Mineral Petrogr Mitt 73: 137–138

Voshage H, Hunziker JC, Hofmann AW, Zingg A (1987) A Nd and Sr isotopic study of the Ivrea Zone, Southern Alps, N Italy. Contrib Mineral Petrol 97: 31–42

Williams IS (1992) Some observations on the use of zircon U-Pb geochronology in the study of granitic rocks. Trans R Soc Edinburgh – Earth Sci 83: 447–458

Williams IS, Buick IS, Cartwright I (1996) An extended episode of early Mesoproterozoic metamorphic fluid flow in the Reynolds Range, central Australia. J Metamorphic Geol 14: 29–47

Woensdregt CF (1992) Computation of surface energies in an electrostatic point charge model. II. Application to zircon ($ZrSiO_4$) Phys Chem Miner 19: 59–69

Wright JE, Shervais JW (1980) Emplacement age of the Balmuccia lherzolite massif, NW Italy. Int Geol Congr 26: 804

Zingg A (1980) Regional metamorphism in the Ivrea Zone (Southern Alps, N Italy): field and microscopic investigations. Schweiz Mineral Petrogr Mitt 60: 153–179

Zingg A (1983) The Ivrea and Strona–Ceneri zones (Southern Alps, Ticino and N Italy): a review. Schweiz Mineral Petrogr Mitt 63: 361–392

Zurbriggen (1996) Crustal genesis and uplift history of the Strona–Ceneri Zone (Southern Alps). A combined petrological, structural, geochemical, isotopic, and paleomagnetic study. Diss philos II faculty, Univ Berne